วิธีเชิงอนุพันธ์อันดับเศษส่วนปรับค่าได้ที่ปรับปรุงแล้วสำหรับการเพิ่มคุณภาพ
ภาพถ่ายทางการแพทย์

นายวศิน ตรังหิรัณยธร

วิทยานิพนธ์นี้เป็นส่วนหนึ่งของการศึกษาตามหลักสูตรปริญญาวิทยาศาสตรมหาบัณฑิต
สาขาวิชาคณิตศาสตร์ประยุกต์และวิทยาการคณนา
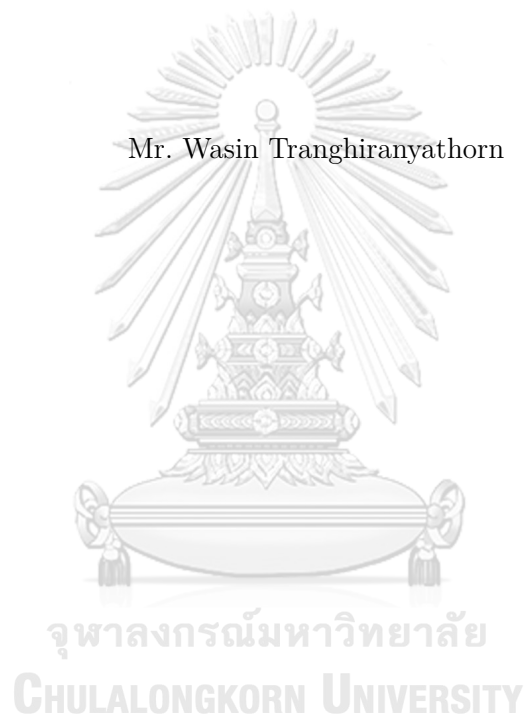ภาควิชาคณิตศาสตร์และวิทยาการคอมพิวเตอร์
คณะวิทยาศาสตร์ จุฬาลงกรณ์มหาวิทยาลัย
ปีการศึกษา 2563

IMPROVED ADAPTIVE FRACTIONAL ORDER DIFFERENTIAL

METHOD FOR MEDICAL IMAGE ENHANCEMENT

Mr. Wasin Tranghiranyathorn

A Thesis Submitted in Partial Fulfillment of the Requirements

for the Degree of Master of Science Program in Applied Mathematics and

Computational Science

Department of Mathematics and Computer Science

Faculty of Science

Chulalongkorn University

Academic Year 2020

Thesis Title	IMPROVED ADAPTIVE FRACTIONAL ORDER DIFFER-ENTIAL METHOD FOR MEDICAL IMAGE ENHANCE-MENT
By	Mr. Wasin Tranghiranyathorn
Field of Study	Applied Mathematics and Computational Science
Thesis Advisor	Associate Professor Ratinan Boonklurb, Ph.D.

Accepted by the Faculty of Science, Chulalongkorn University in Partial Fulfillment of the Requirements for the Master's Degree

. . . . Dean of the Faculty of Science

(Professor Polkit Sangvanich, Ph.D.)

THESIS COMMITTEE

. . . . Chairman

(Associate Professor Petarpa Boonserm, Ph.D.)

. . . . Thesis Advisor

(Associate Professor Ratinan Boonklurb, Ph.D.)

. . . . Examiner

(Associate Professor Khamron Mekchay, Ph.D.)

. . . . External Examiner

(Suriya Natsupakpong, Ph.D.)

วศิน ตรังหิรัณยธร : วิธีเชิงอนุพันธ์อันดับเศษส่วนปรับค่าได้ที่ปรับปรุงแล้วสำหรับการ
เพิ่มคุณภาพภาพถ่ายทางการแพทย์ . (IMPROVED ADAPTIVE FRACTIONAL
ORDER DIFFERENTIAL METHOD FOR MEDICAL IMAGE ENHANCE-
MENT) อ.ที่ปรึกษาวิทยานิพนธ์หลัก : รศ.ดร.รตินันท์ บุญเคลือบ, 51 หน้า.

ในงานนี้เรานำเสนอการสร้างมาสก์เชิงอันดับเศษส่วนขนาด 5×5 โดยอาศัยตัวดำเนินการปรับค่า
ได้ที่ใช้สิบหกทิศทางและถ่วงน้ำหนักพิกเซลแต่ละช่องในมาสก์ด้วยระยะทางแบบยุคลิดจากจุดกึ่งกลาง
ของมาสก์ จากนั้นเรานำมาสก์ใหม่นี้ไปใช้ร่วมกับวิธีอนุพันธ์อันดับเศษส่วนปรับค่าได้ที่ปรับปรุงแล้ว
(AFDA) ซึ่ง AFDA ช่วยให้สามารถหาอันดับเศษส่วนที่เหมาะสมที่สุดของสำหรับพิกเซลแต่ละช่องได้
โดยใช้ฟังก์ชันปรับค่าได้ที่สร้างขึ้นตามสมบัติของส่วนต่าง ๆ ของภาพ ผลการทดลองกับภาพทางการ
แพทย์แสดงให้เห็นว่า AFDA ที่ใช้มาสก์ใหม่ทำการปรับปรุงภาพได้ดีกว่า AFDA แบบดั้งเดิม กล่าว
คือ ทำให้ขอบชัดเจนขึ้น รักษารายละเอียดและปรับปรุงความคมชัดของภาพทางการแพทย์ นอกจากนี้
เรายังใช้มาสก์ที่นำเสนอขึ้นเพื่อคืนสภาพภาพที่เสียหายจากสัญญาณรบกวนแบบเกาส์ เราใช้อัตราส่วน
สัญญาณสูงสุดต่อสัญญาณรบกวน (PSNR) และการวัดดัชนีความคล้ายของโครงสร้าง (SSIM) เพื่อ
ประเมินคุณภาพของการคืนสภาพภาพ การเปลี่ยนค่าของอันดับเศษส่วน ช่วยให้สามารถปรับค่าสัมประสิทธิ์
ของมาสก์สำหรับภาพแต่ละภาพ ตามลักษณะเฉพาะของภาพนั้น ผลการทดลองแสดงให้เห็นว่ามาสก์ที่
นำเสนอมีผลต่อการรักษารายละเอียดของภาพมากกว่าวิธีการคืนสภาพภาพแบบอื่นที่ใช้กันอยู่ทั่วไป
นอกจากนี้ภาพผลลัพธ์ไม่มีความเบลออย่างมีนัยสำคัญซึ่งสามารถบ่งชี้ได้จาก SSIM ที่มีค่ามาก เราสรุป
ว่ามาสก์ที่นำเสนอสามารถปรับปรุงภาพผลลัพธ์ทั้งในแง่การมองเห็นและในแง่ของ PSNR และ SSIM
ได้อย่างมีประสิทธิภาพ

ภาควิชา	คณิตศาสตร์และ	ลายมือชื่อนิสิต ....
	วิทยาการคอมพิวเตอร์	ลายมือชื่อ อ.ที่ปรึกษาหลัก ....
สาขาวิชา	คณิตศาสตร์ประยุกต์	
	และวิทยาการคณนา	
ปีการศึกษา	2563	

6172057423 : MAJOR APPLIED MATHEMATICS AND COMPUTATIONAL SCIENCE

KEYWORDS : ADAPTIVE / FRACTIONAL DIFFERENTIAL / IMAGE ENHANCEMENT

WASIN TRANGHIRANYATHORN : IMPROVED ADAPTIVE FRACTIONAL ORDER DIFFERENTIAL METHOD FOR MEDICAL IMAGE ENHANCEMENT. ADVISOR : ASSOC. PROF. RATINAN BOONKLURB, Ph.D., 51 pp.

In this work, we propose a construction of a new 5×5 fractional order differential mask that uses sixteen directions of gradient operator and weights each pixel in the mask by the Euclidean distance from the center of the mask. Then, we apply this new mask to the Adaptive Fractional Differential Algorithm (AFDA). The AFDA allows the optimal fractional order of each pixel to be obtained using an adaptive function constructed based on the area feature of image. Experimental results for medical images, show that the AFDA with the new mask gives better image enhancement than the original AFDA. It makes edges clearer, preserving texture details and improving the contrast of medical images. Moreover, we also use the proposed mask to restore the noisy images which are corrupted by the Gaussian noise. We use the peak signal to noise ratio (PSNR) and the structural similarity index measure (SSIM) to evaluate the quality of the denoised images. Changing the values of the fractional orders allows adjusting the mask coefficients for each image according to it characteristics. The experiments provide that the proposed mask has an influence on preserving more texture detail than the common used denoising filters. In addition, the output images have no significant blurring which can be indicated by higher SSIM. We conclude that the proposed mask can improve the result visually and in terms of PSNR and SSIM efficiently.

Department   : Mathematics and Computer Science   Student's Signature ....

Field of Study   : Applied Mathematics and Computational Science   Advisor's Signature ....

Academic Year : 2020

ACKNOWLEDGEMENTS

CONTENTS

LIST OF TABLES

LIST OF FIGURES

CHAPTER I

INTRODUCTION

This chapter describes the motivation of this research, problems of previous works and the scope of this research.

1.1 Motivation

Medical image quality has become an indispensable part of modern medicine and directly influences the accuracy of doctors' diagnoses and treatments. Low resolution and low contrast in medical images have made correct diagnosis difficult; this directly influences the speed and accuracy of doctor's diagnoses. Therefore, it is necessary to improve medical image enhancement to reflect the information of an illness more clearly and accurately, for more details see [1], [2] and [3].

Fractional differential, which is a theory of arbitrary order derivatives, is generalized from integral order differential (see [4] and [5] for definitions and properties). Compared with integral order differential approaches, fractional differentials applied to image processing can enhance edges, make texture details clearer and preserve smooth areas (see [6], [7] and [8].) Moreover, fractional derivatives for image denoising problems have also been considered in [9] and [10].

Traditional fractional differentials use the same fractional order to process edges, textures and smooth areas of image; however, while edges would be enhanced by high fractional orders, weak textures and smooth areas would be ignored while, weaker textures and smoother areas would be preserved by low fractional orders, edges would be weakened. Thus, image enhancement is difficult to attain in practice. To handle with these issues, traditional fractional differential algorithms have been developed for digital image processing in [11], [12], [13] and [14]. Especially, in 2015, Li and Xie [15] proposed

the Adaptive Fractional Differential Algorithm (AFDA) for medical image enhancements that can extract the edges of an image accurately and enhance them while preserving smooth areas and weak textures. It is an evidence that the AFDA gives better results comparing with the existing methods, namely the histogram equalization algorithm, Sobel, Laplacian, traditional fractional differential methods, which are 0.5-order, 0.8-order and 1-order, respectively.

1.2 Objectives

In this work, we propose a construction of the new 5×5 fractional order differential mask that uses sixteen directions of gradient operator and weights each pixel in the mask by the Euclidean distance from the center of the mask to reduce the over-valuation of the gradient from distant pixels to improve the AFDA that proposed by Li and Xie [15]. Then, we evaluate the effect of the image enhancement by visual analysis, quality of the edge detection and some metrics and compare the results with the original AFDA. Moreover, we use the proposed 5×5 fractional differential mask to restore the noisy images which are corrupted by the Gaussian noise to provide other evidence that the proposed mask has an influence on preserving more texture detail than the traditional denoising filters which contain a mean filter, a Gaussian filter and a Weiner filter. To validate the performance, we use the peak signal to noise ratio (PSNR) and the structural similarity index measure (SSIM) to evaluate the quality of the denoised images.

1.3 Thesis Overview

The remainder of this thesis is organized as follows. In Chapter II, we present some necessary related background knowledge using in this work. Chapter III presents a construction of the new 5×5 fractional differential mask, discusses the experiments and comparisons, and presents conclusions. Chapter IV demonstrates the results of a denoising algorithm using the proposed filter comparing with existing common used filters. The discussions and conclusions are provided.

CHAPTER II

BACKGROUND KNOWLEDGE

The purpose of this chapter is to recall the necessary theoretical and mathematical background about an image processing and fractional order derivative which will be used in this research.

2.1 Digital image processing

Digital image processing is a method to perform some algorithms or some techniques on an image in order to get an enhanced image or to extract some useful information from it by using a digital computer to process. There are several applications in digital image processing such as industry, agriculture, military, robotics, remote sensing, and medical diagnosis [16].

2.1.1 Digital image definition

A digital image is defined via a two-dimensional function, $f(x, y)$, where x and y are discrete coordinates, and the value of f at any coordinates (x, y) is called the intensity or gray level of the image at that point.
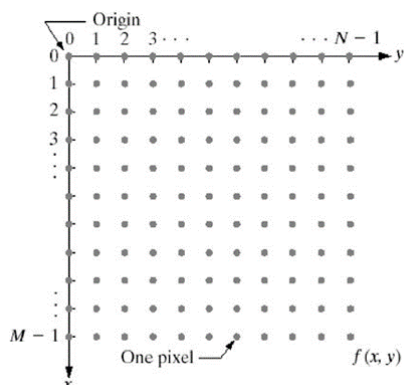
Figure 2.1: The coordinate convention used

Assume that an image f is considered over M rows and N columns of two-dimensional XY-plane, shown in Figure 2.1. If the integer values are assigned for these discrete coordinates as: $x = 0, 1, 2, ..., M-1$ and $y = 0, 1, 2, ..., N-1$, then the image f can be written in the matrix form

$$f = \begin{bmatrix} f(0,0) & f(0,1) & \dots & f(0,N-1)) \\ f(1,0) & f(1,1) & \dots & f(1,N-1)) \\ \vdots & \vdots & \ddots & \vdots \\ f(M-1,0) & f(M-1,1)) & \dots & f(M-1,N-1) \end{bmatrix}.$$

Each element of this matrix is called a pixel or an image element or an image intensity.

2.1.2 Grayscale image

A grayscale image is simply one in which the only colors are shades of gray. The intensity is stored as an 8-bit integer giving 256 possible different shades of gray from black to white. Therefore, the range of pixels is 0–255. All shades of gray are shown in Figure 2.2.
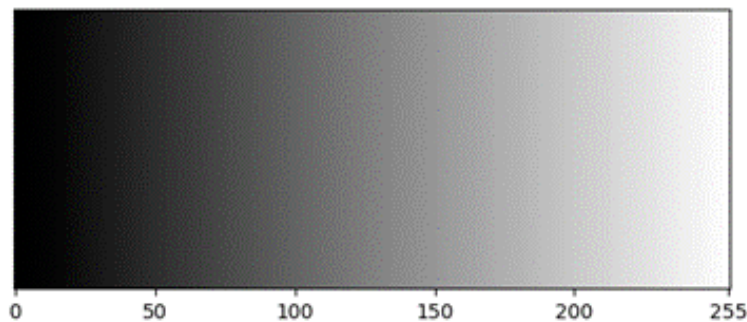
Figure 2.2: The 256 intensity levels for an 8-bit shades of gray

2.2 Kernel, convolution and normalization

In image processing, a kernel is a matrix of real numbers [16]. It is invaluable to image processing techniques. It can be use for blurring, edge detection and sharpening.
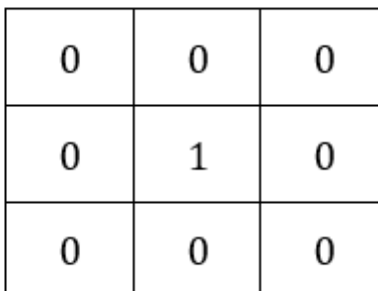
In literature, this type of kernel maybe referred as a spatial kernel or mask or filter or window. However, we use mask in Chapter III and use filter in Chapter IV of this thesis.

Convolution is a process of transforming an image by applying a kernel over each pixel where the kernel lies entirely inside the image region and its local neighbors across the entire image. The convolution process involves these steps. It places the kernel matrix over each pixel of the image, multiplies each value of the kernel with the corresponding pixel. Then, sums the resulting multiplied values and returns the resulting value as the new value of the center pixel. This process is repeated across the entire image. The general expression of a convolution at a coordinate (x, y) of an image f is

$$g(x, y) = \omega * f(x, y) = \sum_{s=-a}^{a} \sum_{t=-b}^{b} \omega(s, t) f(x + s, y + t),$$

where g is the filtered image and ω is the kernel of size $(2a + 1) \times (2b + 1)$.

For example, an identity kernel shown in Figure 2.3, when applied to an image through convolution, will have no effect on the resulting image. Every pixel will retain its original value.

0	0	0
0	1	0
0	0	0

Figure 2.3: Identity kernel

Normalization is defined as the division of each element in the kernel by the sum of all kernel elements, so that the sum of the elements of a normalized kernel is unity. To ensure that the average pixel in the processed image is as bright as the average pixel in the original image.

2.3 Image smoothing

Image smoothing is a digital image processing technique that reduces and suppresses image noises [16]. In the spatial domain, neighborhood averaging can generally be used to achieve the purpose of smoothing. In literature, if one consider image smoothing, then the followings are the commonly used filters for each technique.

2.3.1 Mean filter

The mean filter is a filter that all coefficients values have the same weight and replaces the center value in the filter with the average of all pixel values in the filter. The mean filter is also called a box filter. The mean filter simply smoothes or blurs local variations in an image. Noise is reduced from an original image as a result of convolution the original image with the mean filter.
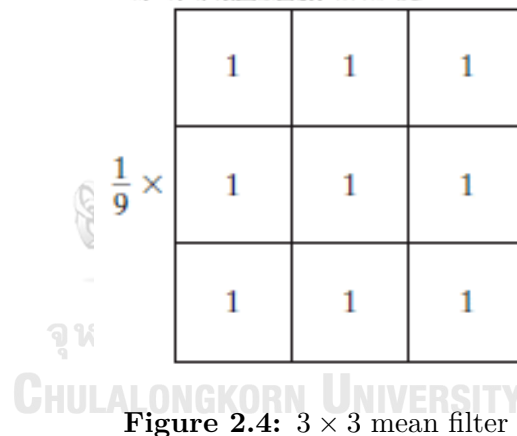
Figure 2.4: 3×3 mean filter

Figure 2.4 shows 3×3 mean filter. In general, an $m \times n$ mean filter has $1/mn$ as its normalizing constant.

2.3.2 Gaussian filter

Gaussian filter is a filter commonly used in image processing for smoothing and reducing noise of an image. Gaussian filter has the shape of the Gaussian distribution

and define the coefficients inside the filter of the form

$$G(x,y) = \frac{1}{2\pi\sigma^2} e^{-\frac{x^2+y^2}{2\sigma^2}},$$

where x is the horizontal distance from the origin of the filter, y is the vertical distance from the origin of the filter and σ is the standard deviation of the Gaussian distribution with mean $(0,0)$. The Gaussian distribution over $[-3,3]^2$ with $\sigma = 1$ is shown in Figure 2.5. A 5×5 Gaussian filter with $\sigma = 1$ is shown in Figure 2.6.
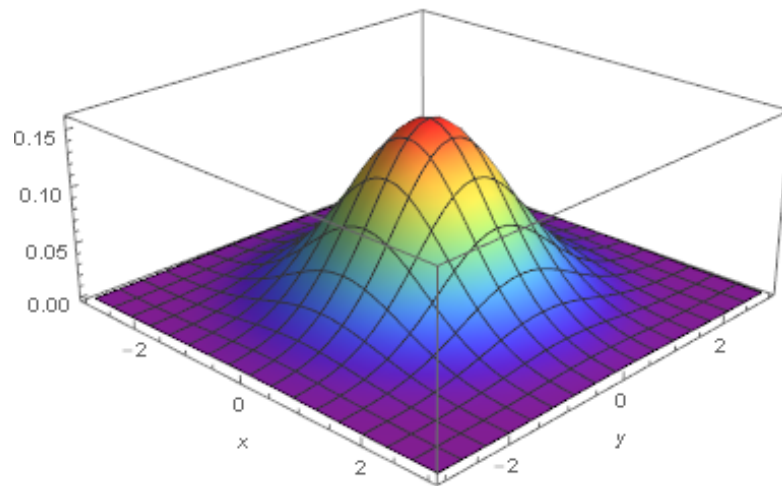
Figure 2.5: Gaussian distribution with mean $(0,0)$ and $\sigma = 1$

Figure 2.6: 5×5 Gaussian filter with $\sigma = 1$
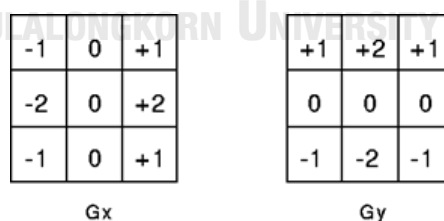
The center pixel's value receives the heaviest weight and neighboring pixels receive smaller weights as their distance to the center pixel increases. This results in a blur that preserves boundaries and edges better than other filters with more uniform weight.

2.4 Image sharpening

Image sharpening is a digital image processing technique that sharpen and highlight the edges [16]. It enhances the grayscale transition of an image, which is the opposite process of image smoothing. While, image smoothing is based on the weighted summation or integral operation on the neighborhood, the sharpening is based on the derivative (gradient) or finite difference. In image smoothing, we try to smooth the noise and ignore edges, but in sharpening, we try to enhance edges and ignore the noise. In literature, if one consider image sharpening, then the followings are the commonly used filters for each technique.

2.4.1 Sobel filter

The Sobel filter performs a two-dimensional spatial gradient measurement on an image and is used for edge detection. Typically, it is used to find the approximate absolute gradient magnitude at each point in an input grayscale image. The Sobel filters consist of a pair of 3×3 matrices as shown in Figure 2.7.
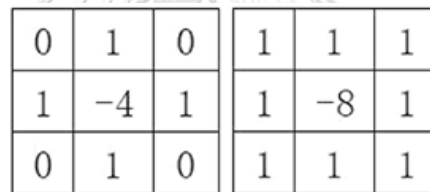
Figure 2.7: Sobel filters in x and y directions

These filters are designed to respond the edges vertically and horizontally relative to the pixel grid. Note that the sums of coefficients in both filters are 0, indicating that they would give a response of 0 in an area of constant gray level, as expected for a derivative operator. The filters can be applied separately to the input image, to produce

separate measurements of the gradient component in each orientation, namely Gx and Gy. Moreover, it can be combined to find the absolute magnitude of the gradient at each point which is given by $|G| = \sqrt{Gx^2 + Gy^2}$. Typically, an approximate magnitude is computed using $|G| = |Gx| + |Gy|$ which is much faster to compute.

2.4.2 Laplacian filter

The Laplacian filter is a isotropic matrix that measure of the second spatial derivative of an image. It tries to highlight regions of rapid intensity change. It helps to find out whether the changes we are observing are due to pixel change of continuous regions or from an edge. The Laplacian filter of a pixel $f(x, y)$ is defined as $\nabla^2 f = \frac{\partial^2 f}{\partial x^2} + \frac{\partial^2 f}{\partial y^2}$. Two commonly used discrete approximations to the Laplacian filter are shown in Figure 2.8.

0	1	0
1	−4	1
0	1	0

1	1	1
1	−8	1
1	1	1

Figure 2.8: Two commonly used discrete approximations to the Laplacian filter

2.5 Gaussian noise

Noise is basically a disturbance that distorts the information presented in the image [16]. It is usually an unwanted signal that can create a variation in image intensity levels of pixels which cause degradation of image quality. There are many types of noises occurs in images, especially, medical images. One of the mostly occurred noise is the Gaussian noise.

Gaussian noise involves a Gaussian distribution or a bell shaped distribution. The probability density function p_G of a Gaussian random variable z is given by

$$p_G(z) = \frac{1}{\sigma\sqrt{2\pi}} e^{-\frac{(z-\mu)^2}{2\sigma^2}},$$

where z represents the grayscale value, μ is the mean of the grayscale value and σ is the standard deviation of the noise. An example of an image with Gaussian noise is shown in Figure 2.9(b).
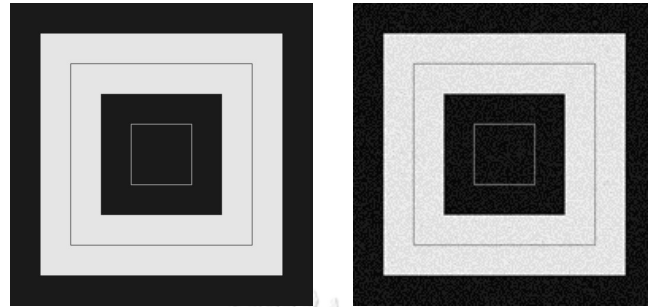
(a) Without noise (b) With Gaussian noise

Figure 2.9: A Noise-free image and an image with Gaussian noise

2.6 Fractional calculus

2.6.1 Definitions of fractional order derivative

There are three classical definitions of fractional calculus, namely, the Grünwald–Letnikov (G-L) definition, the Riemann–Liouville (R-L) definition and the Caputo definition. The G-L definition is deduced from the expression of integer-order differential, whereas the R–L and Caputo definitions are derived from integer-order Cauchy integral formula. Since the G–L definition is less complex than the others and only uses one coefficient, the G–L definition is suitable for signal processing and it is the most popular definition used in digital image processing [4].

Let $v \in \mathbb{R}^+$. Considering a function $f(t)$ on an interval $[a, b]$ which has m-order $(m = \lceil v \rceil)$ continuously differentiable. The v-order (G-L) fractional derivative of $f(t)$ is defined by

$$_aD_b^v f(t) = \frac{d^v f(t)}{dt^v} = \lim_{h \to 0} h^{-v} \sum_{j=0}^{[(b-a)/h]} (-1)^j \binom{v}{j} f(t - jh), \qquad (2.1)$$

where [ ] is the integral part and $\binom{v}{j}$ is the binomial coefficient.

For a small value of h, (2.1) can be approximated by

$$\frac{d^v f(t)}{dt^v} \approx h^{-v} \left(f(t) + (-v)f(t-h) + \frac{(-v)(-v+1)}{2}f(t-2h) + \cdots + \frac{\Gamma(-v+1)}{n!\Gamma(-v-n+1)}f(t-nh) \right),$$

where Γ is the gamma function.

In term of image processing, we usually let $h = 1$. When the interval $[a, b]$ of $f(t)$ is divided into equal parts by taking the duration of $h = 1$, then $n = [(b-a)/h] = [b-a]$ and the v-order fractional differential of $f(t)$, $_aD_b^v f(t)$, can be approximated by

$$\frac{d^v f(t)}{dt^v} \approx f(t) + (-v)f(t-1) + \frac{(-v)(-v+1)}{2}f(t-2) + \cdots + \frac{\Gamma(-v+1)}{n!\Gamma(-v-n+1)}f(t-n) \quad (2.2)$$

.

2.6.2 Realization of fractional differential masks

For $f(x, y)$ in the region $[a, b] \times [c, d]$, we can extend (2.2) to obtain the backward difference of the v-order fractional partial differentials on the x- and negative y-coordinates, respectively, as

$$\frac{\partial^v f(x,y)}{\partial x^v} \approx f(x, y) + (-v)f(x-1, y) + \frac{(-v)(-v+1)}{2}f(x-2, y) + \cdots + \frac{\Gamma(-v+1)}{n!\Gamma(-v-n+1)}f(x-n, y) \quad (2.3)$$

$$\frac{\partial^v f(x,y)}{\partial y^v} \approx f(x, y) + (-v)f(x, y-1) + \frac{(-v)(-v+1)}{2}f(x, y-2) + \cdots + \frac{\Gamma(-v+1)}{m!\Gamma(-v-m+1)}f(x, y-m), \quad (2.4)$$

where $n = [b - a]$ and $m = [d - c]$. Figure 2.10 shows the 3×3 partial fractional order differential masks of the x- and y-axes which can be obtained from the first three coefficients of (2.3) and (2.4), namely $1, -v$ and $\frac{v^2 - v}{2}$.

Additionally, Li and Xie [15] can obtained eight masks in each direction (i.e., 0°, 45°, 90°, 135°, 180°, 225°, 270°, and 315°) and the 5×5 mask of eight directions shown in Figure 2.11 is obtained by rotation and superimposing them. Each pixel of Figure 2.11 must be divided by $8 \times (1 + (-v) + (v^2 - v)/2) = 8 - 12v + 4v^2$ to acquire the final 5×5 fractional order differential mask. Finally, they used the final 5×5 fractional order

				$\dfrac{v^2 - v}{2}$	
$\dfrac{v^2 - v}{2}$	$-v$	1		$-v$	
				1	

Figure 2.10: 3×3 partial fractional order differential masks of the x- and y-axes

differential mask to process the medical images.

$\dfrac{v^2 - v}{2}$	0	$\dfrac{v^2 - v}{2}$	0	$\dfrac{v^2 - v}{2}$
0	$-v$	$-v$	$-v$	0
$\dfrac{v^2 - v}{2}$	$-v$	1×8	$-v$	$\dfrac{v^2 - v}{2}$
0	$-v$	$-v$	$-v$	0
$\dfrac{v^2 - v}{2}$	0	$\dfrac{v^2 - v}{2}$	0	$\dfrac{v^2 - v}{2}$

Figure 2.11: 5×5 fractional order differential mask

2.6.3 Adaptive fractional differential function

According to Li and Xie [15], they proposed the adaptive order v of fractional order differential where $v \in [0, 1]$ and (i, j) is a coordinate in the region of an image f of size $m \times n$ as

$$v = \begin{cases} \frac{M(i,j)-t}{M(i,j)} & \text{if } M(i,j) \geq t \text{ and } \frac{M(i,j)-t}{M(i,j)} \geq v_1 \\[2mm] v_1 & \text{if } M(i,j) \geq t \text{ and } \frac{M(i,j)-t}{M(i,j)} < v_1 \\[2mm] v_2 & \text{if } 2 < M(i,j) < t \text{ and } \frac{M(i,j)}{t} \geq v_2 \\[2mm] \frac{M(i,j)}{t} & \text{if } 2 < M(i,j) < t \text{ and } \frac{M(i,j)}{t} < v_2 \\[2mm] 0 & \text{if } 0 \leq M(i,j) \leq 2 \end{cases}, \qquad (2.5)$$

where

$$M(i,j) = \frac{|8f(i,j)-f(i-1,j-1)-f(i-1,j)-f(i-1,j+1)-f(i,j-1)-f(i,j+1)-f(i+1,j-1)-f(i+1,j)-f(i+1,j+1)|}{8}$$

is the average gradient of pixel $f(i,j)$, t is the gradient threshold, v_1 and v_2 are the thresholds of order which are defined by

$$v_1 = \frac{M_{ed} - Q}{M_{ed}} \text{ and } v_2 = \frac{Q - M_{tex}}{Q}. \tag{2.6}$$

Here, the parameter Q is the average gradient of the original image which is defined by

$$Q = \sum_{i=1}^{m-1} \sum_{j=1}^{n-1} \sqrt{\frac{(f(i,j)-f(i+1,j))^2 + (f(i,j)-f(i,j+1))^2}{2}},$$

M_{ed} and M_{tex} are the average gradients of edges pixels and texture pixels segmented by Otsu algorithm, respectively. Moreover, they determined threshold t via the improved Otsu algorithm which will be elaborated in Section 2.7.

This adaptive order v conditionally determined by $M(i,j)$ the average gradient of each pixel to be greater or less than the threshold t to classify a pixel as an edge or texture, if $0 \leq M(i,j) \leq 2$, this pixel is defined as a smooth area. In addition, there is also an order value condition, with order v_1 categorizing it as a group of strong or weak edges and order v_2 as a classifying of a strong or weak texture group

2.7 Thresholding

In digital image processing, thresholding is a method of segmenting images which aim to partition each pixels of an image into foreground and background [17]. For a grayscale image, simple thresholding can be used to create binary images by selecting some fixed constant T. We replace each pixel in an image with a black pixel if the image intensity $f(x,y)$ is less than T or by a white pixel if the image intensity $f(x,y)$ is greater than or equal that constant. For each (x,y) in the region of an image f, the segmented

image using the simple thresholding with constant T, denoted by $g(x, y)$, is defined as

$$g(x, y) = \begin{cases} 1 & \text{if } f(x, y) \geq T, \\ 0 & \text{if } f(x, y) < T. \end{cases}$$

A problem with simple thresholding is that you have to manually specify the threshold constant. We can manually check how good a threshold is by trying different values. However, it is very slow and may break down in the real world. Thus, we need a way to automatically determine the threshold. The Otsu's method is one of a good example of the auto thresholding.

The Otsu's method was proposed by Otsu [17]. It is used to perform an automatic image thresholding. This algorithm returns an optimal threshold constant that separate pixels into two classes, foreground and background. By going through all possible threshold values, it finds the optimal threshold value of input image by minimizing intra-class intensity variance, or equivalently, by maximizing inter-class variance.

Let t be an integer in $[0, 255]$. Suppose a grayscale image f has n distinct integer intensity values. The intra-class variance using a threshold constant t, denoted by $\sigma_\omega^2(t)$, is defined as a weighted sum of variances of the two classes. That is

$$\sigma_\omega^2(t) = \omega_1(t)\sigma_1^2(t) + \omega_2(t)\sigma_2^2(t),$$

where $\omega_1(t)$ and $\omega_2(t)$ are the probabilities of the two classes divided by a threshold constant t, and $\sigma_1^2(t)$ and $\sigma_2^2(t)$ are variances of these two classes.

The quantity of the pixels with a specified grayscale value i denotes by n_i. Since there are n values of pixel intensity in the image, the probability of the grayscale value i occurrence is

$$p(i) = \frac{n_i}{n}.$$

The threshold constant t separates the pixel intensity values into two classes: $C_1 =$

$\{0, 1, 2, \ldots, t\}$ and $C_2 = \{t + 1, t + 2, t + 3, \ldots, I\}$, where I is the maximum pixel value.

The class probabilities $\omega_1(t)$ and $\omega_2(t)$ are computed by

$$\omega_1(t) = \sum_{i=0}^{t} p(i) \text{ and } \omega_2(t) = \sum_{i=t+1}^{I} p(i).$$

The next step is to obtain the class means for C_1 and C_2, which are denoted by $\mu_1(t)$ and $\mu_2(t)$, respectively. That is

$$\mu_1(t) = \sum_{i=0}^{t} \frac{ip(i)}{\omega_1(t)} \text{ and } \mu_2(t) = \sum_{i=t+1}^{I} \frac{ip(i)}{\omega_2(t)}.$$

Thus, the total mean μ_T is given by

$$\mu_T = \mu_1(t)\omega_1(t) + \mu_2(t)\omega_2(t) = \sum_{i=0}^{I} ip(i).$$

Then, we have the class variances for C_1 and C_2, which are denoted by $\sigma_1^2(t)$ and $\sigma_2^2(t)$, respectively. That is

$$\sigma_1^2(t) = \sum_{i=0}^{t} (i - \mu_1(t))^2 \frac{p(i)}{\omega_1(t)} \text{ and } \sigma_2^2(t) = \sum_{i=t+1}^{I} (i - \mu_2(t))^2 \frac{p(i)}{\omega_2(t)}.$$

Finally, the optimal threshold constant t^* is obtained by minimizing the intra-class variance $\sigma_\omega^2(t)$. That is

$$t^* = \operatorname*{argmin}_{0 \leq t \leq I} \sigma_\omega^2(t).$$

Note that for 2 classes, if $\sigma_b^2(t)$ is inter-class variance, then

$$\sigma_b^2(t) = \sigma^2 - \sigma_\omega^2(t) = \omega_1(t)(\mu_1(t) - \mu_T)^2 + \omega_2(t)(\mu_2 - \mu_T)^2 = \omega_1(t)\omega_2(t)(\mu_1(t) - \mu_2(t))^2.$$

Thus, minimizing the intra-class variance $\sigma_\omega^2(t)$ is equivalent to maximizing inter-class variance $\sigma_b^2(t)$. The desired threshold t^* also corresponds to the maximum $\sigma_b^2(t)$.

Li and Xie [15] improved the traditional Otsu algorithm to obtain an improved

image enhancement effect for AFDA, by replacing the grayscale value of each pixel $f(i,j)$ with the average gradient $M(i,j)$. This improved Otsu algorithm can segment edges, textures and smooth areas of an image more effectively. Considering the integer portion of $M(i,j)$ belongs to $\{0, 1, 2, \ldots, k, \ldots, N(i,j)\}$, the threshold t divides the image gradient into two parts: $C_1 = \{1, 2, 3, \ldots, t\}$ and $C_2 = \{t+1, t+2, t+3, \ldots, \max(N(i,j))\}$. The gradient threshold t divides the gradient image into an edge and a background.

2.8   Performance evaluation metrics

To evaluate the performance of the image processing techniques, we have several metrics to indicate. The following are metrics that will be used in this thesis [18], [19], [20].

2.8.1   Peak signal-to-noise ratio (PSNR)

PSNR is the ratio between the maximum possible value (or power) of a signal and the power of distorting noise that affects the quality of its representation. Note that, in image processing, signal refers to an image f.

Given a noise-free $m \times n$ monochrome image f and its degraded image g, the mean squared error (MSE) is defined by

$$MSE = \frac{1}{mn} \sum_{i=0}^{m-1} \sum_{j=0}^{n-1} (f(i,j) - g(i,j))^2.$$

MSE represents the average of the squares of the difference between our actual image and our degraded image.

PSNR is defined by

$$PSNR = 10 \log_{10} \frac{MAX_f^2}{\sqrt{MSE}},$$

where MAX_f is the maximum possible pixel value of the noise-free image f.

The idea is that the higher the PSNR, the better the degraded image has been

reconstructed to match the original image and the better the algorithm. This would occur because we wish to minimize the MSE between images with respect to the maximum intensity value of the image.

When we compute the MSE between two identical images, the value will be zero and hence the PSNR will be undefined. The main limitation of this metric is that it relies strictly on numeric comparison and does not actually take into account any level of biological factors of the human vision system unlike the structural similarity index measure.

2.8.2 Structural similarity index measure (SSIM)

SSIM is an image quality metric that assesses the visual impact of three characteristics of an image, namely, luminance (l), contrast (c) and structure (s). The index is a multiplicative combination of the three terms. That is

$$SSIM(f,g) = (l(f,g))^{\alpha}(c(f,g))^{\beta}(s(f,g))^{\gamma},$$

where

$$l(f,g) = \frac{2\mu_f\mu_g + C_1}{\mu_f^2 + \mu_g^2 + C_1},$$

$$c(f,g) = \frac{2\sigma_f\sigma_g + C_2}{\sigma_f^2 + \sigma_g^2 + C_2} \text{ and}$$

$$s(f,g) = \frac{\sigma_{fg} + C_3}{\sigma_f\sigma_g + C_3}.$$

Here, $\mu_f, \mu_g, \sigma_f, \sigma_g$ and σ_{fg} are the local means, standard deviations and covariance for images f and g. The default for exponents α, β and γ are 1 and the default selection of $C_3 = C_2/2$. Then, the index can be simplified to

$$SSIM(f,g) = \frac{(2\mu_f\mu_g + C_1)(2\sigma_f\sigma_g + C_2)}{(\mu_f^2 + \mu_g^2 + C_1)(\sigma_f^2 + \sigma_g^2 + C_2)}.$$

Usually, the default setting for C_1 and C_2 is $C_1 = (0.01L)^2$ and $C_2 = (0.03L)^2$, where L is the dynamic range of the pixel values and the default dynamic range is 255 for images

of data type uint8. Two variables C_1 and C_2 are introduced to stabilize the division with weak denominator or to avoid instability for image regions where the local mean or standard deviation is close to zero.

The value of SSIM is in the range $[0, 1]$. The value 1 indicates the highest quality and occurs when images f and g are equivalent. Smaller values correspond to poorer quality. SSIM is used for measuring the similarity between two images.

2.8.3   Entropy of information

Entropy is a measure of image information content, which is interpreted as the average uncertainty of information source. It is used in the quantitative analysis and evaluation image details. The entropy value is used as it provides better comparison of the image details. The higher value of entropy implies more detailed information. In image processing, the entropy is defined by

$$H = -\sum_{k=0}^{255} p(k) \ln p(k),$$

where $p(k)$ is the frequency of grayscale values, i.e., $p(k) = \frac{1}{m \times n} \sum_{f(i,j)=k} 1$ for a digital image f with size $m \times n$.

From these background knowledge, we will apply them suitably in Chapters III and IV thereafter.

CHAPTER III

IMPROVED MASK FOR ADAPTIVE FRACTIONAL ORDER DIFFERENTIAL METHOD FOR MEDICAL IMAGE ENHANCEMENT

This chapter describes a construction of the new 5×5 fractional order differential mask. Then, we apply this new mask to the Adaptive Fractional Differential Algorithm (AFDA) to enhance the medical images.

3.1 An improved fractional differential mask

In this section, we describe how to construct a new fractional differentiation mask and point out the advantages of the proposed mask. In order to strengthen the anti-rotation performance of the Adaptive Fractional Differential Algorithm (AFDA), sixteen directions of the gradient operator are used to construct the new 5×5 fractional differential mask. First, Figure 3.1(a) shows a 0° direction of the gradient. Next, in Figure 3.1(b), we add a 22.5° direction (red dashed line). Here, we notice that the red dashed line passes through two pixels of the level of $-v$. Thus, we divide these $-v$ neighbors into two equal parts. After superimposing the gradient operator in 45° direction, the mask becomes Figure 3.1(c). We repeat this process until we get a full cycle as shown in Figures 3.1($d-h$). Figure 3.1(i) shows the 5×5 mask of sixteen directions which is obtained by the sum of every value in each pixel of Figure 3.1(h).

To reduce the over-valuation of the gradient from distant pixels, we weight each pixel in the mask by the Euclidean distance from the center of the mask. Consider Figure 3.1(j). First, we label the center of the mask with ''0''. Second, we label the layer of $-2v$ with ''1'' and ''1'''. Third, we label the layer of $(v^2 - v)/2$ with ''2'', ''2''' and ''2''''. In

Figure 3.1(j), the pixels labeled by "1" and "1′" are 1 and $\sqrt{2}$ unit away from the center, respectively. Therefore, we weight the gradient of 1-pixels and 1′-pixels with 1/1 and $1/\sqrt{2}$, respectively, to decrease their values as shown in Figure 3.1(k). In Figure 3.1(j), the pixels labeled by "2", "2′" and "2″" are 2, $\sqrt{5}$ and $2\sqrt{2}$ unit away from the center, respectively. Therefore, we weight the gradient of 2-pixels, 2′-pixels and 2″-pixels with $2/2$, $2/\sqrt{2}$ and $2/(2\sqrt{2})$, respectively, to decrease their values as shown in Figure 3.1(k). Next, we multiply each pixel of Figure 3.1(i) by each pixel of Figure 3.1(k) componentwise to obtain our new 5×5 weighted fractional differential mask of sixteen directions as shown in Figure 3.1(l). Finally, we divide each pixel of Figure 3.1(l) by the sum of all values in the mask, $S = 16 + (-10 - 5\sqrt{2} - 8\sqrt{5}/5)v + (2 + \sqrt{2} + 8\sqrt{5}/5)v^2$. Note that S has no real root which implies that the denominator cannot be zero.

3.2 Experimental Results and Discussion

We choose four medical images as shown in Figures 3.3(a) – 3.6(a) to represent common medical images. Figure 3.3(a) shows an image of ultrasound in pregnancy. Figure 3.4(a) shows a lung sectional CT image, Figure 3.5(a) shows a knee-joint MRI and Figure 3.6(a) shows a target of breast molybdenum image, respectively. The resolutions of all images are 256×256 and the gradient threshold t of these four original images can be obtained by using the improved Otsu algorithm [15]. The parameters v_1, v_2 and t for each image are shown in Table 3.1. The effect of image enhancement is evaluated by visual analysis, quality of the edge detection and some metrics. Here, the procedure as shown in Figure 3.2 given by Li and Xie [15] is used by changing the 5×5 fractional order differential mask of eight directions to the one of sixteen directions. The procedure to enhance the original image can be written in a flow chart as shown in Figure 3.2.

Image	v_1	v_2	t
Ultrasonic image	0.7283	0.2406	5
CT image	0.7070	0.2875	13
MRI image	0.7324	0.2395	6
Target of breast molybdenum image	0.7514	0.2283	4

Table 3.1: Parameters of these four images
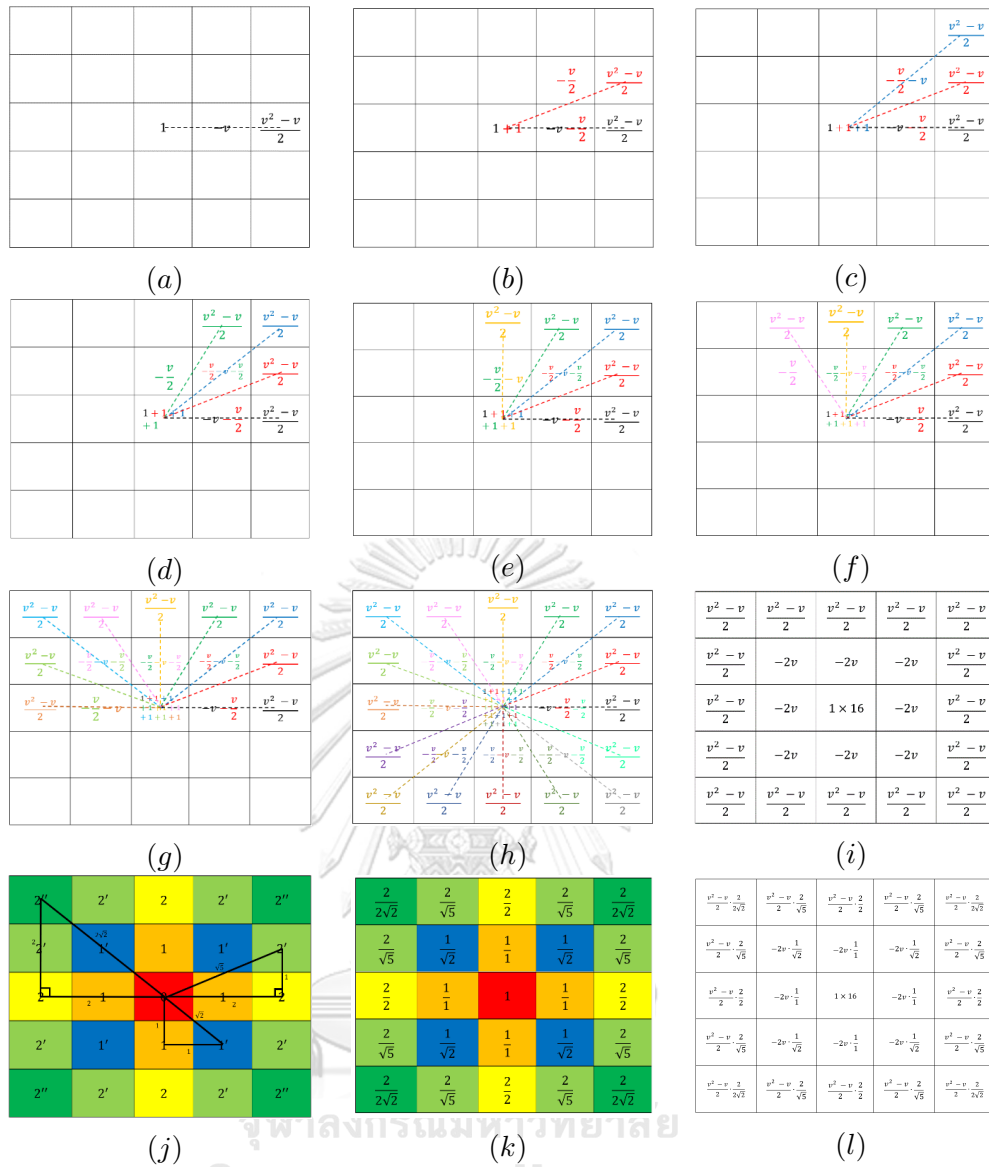
Figure 3.1: Construction of new fractional differential mask

According to Li and Xie [15], the effect of image enhancement of the original AFDA was better when compared with those of the histogram equalization algorithm, Sobel, Laplacian, traditional fractional differential methods, which are 0.5-order, 0.8-order and 1-order, respectively. The results of the histogram equalization method which improve the brightness of the object. However, the local texture details are disappeared and the grays change unnaturally. The results of the traditional fractional differential methods. The 0.5-order method enhances edges and preserve some local texture details while the 0.8-order method strongly enhances edges but produces significantly more noise. The 1-

Start

Input an image I

Resize the input image I to 256×256 and convert to gray scale image.

Find $M(i,j)$ the average gradients of each pixel in eight directions and calculate a parameter Q the average gradient of the original image.

Find the optimal threshold t via the improved Otsu algorithm by replacing the gray level of each pixel $I(i,j)$ of the traditional Otsu algorithm with the integer portion of average gradient $M(i,j)$ belongs to $\{0,1,2,\ldots,N(i,j)\}$. Note that the threshold t can divides the image gradient into two parts

$$\underbrace{C_1 = \{1,2,3,\ldots,t\}}_{\text{Textures and smooth areas}} \quad \text{and} \quad \underbrace{C_2 = \{t+1,t+2,t+3,\ldots,\max(N(i,j))\}}_{\text{Edges}}.$$

Output the threshold t, M_{ed} and M_{tex} the average gradients of edges pixels and texture pixels segmented by Otsu algorithm, respectively.

Calculate parameters v_1 and v_2 defined as $v_1 = \frac{M_{ed}-Q}{M_{ed}}$ and $v_2 = \frac{Q-M_{tex}}{Q}$.

Create a matrix V that keeps the values of adaptive v-order fractional differential function at pixel (i,j) by

$$V(i,j) = \begin{cases} \frac{M(i,j)-t}{M(i,j)} & ; \ M(i,j) \geq t \text{ and } \frac{M(i,j)-t}{M(i,j)} \geq v_1 & \textbf{strong edge} \\ v_1 & ; \ M(i,j) \geq t \text{ and } \frac{M(i,j)-t}{M(i,j)} < v_1 & \textbf{weak edge} \\ v_2 & ; \ 2 < M(i,j) < t \text{ and } \frac{M(i,j)}{t} \geq v_2 & \textbf{strong texture} \\ \frac{M(i,j)}{t} & ; \ 2 < M(i,j) < t \text{ and } \frac{M(i,j)}{t} < v_2 & \textbf{weak texture} \\ 0 & ; \ 0 \leq M(i,j) \leq 2 & \textbf{smooth area} \end{cases}$$

Create the 5×5 fractional order differential mask

$\frac{v^2-v}{2}\frac{1}{\sqrt{2}}$	$\frac{v^2-v}{2}\frac{2}{\sqrt{5}}$	$\frac{v^2-v}{2}$	$\frac{v^2-v}{2}\frac{2}{\sqrt{5}}$	$\frac{v^2-v}{2}\frac{1}{\sqrt{2}}$
$\frac{v^2-v}{2}\frac{2}{\sqrt{5}}$	$-\sqrt{2}v$	$-2v$	$-\sqrt{2}v$	$\frac{v^2-v}{2}\frac{2}{\sqrt{5}}$
$\frac{v^2-v}{2}$	$-2v$	1×16	$-2v$	$\frac{v^2-v}{2}$
$\frac{v^2-v}{2}\frac{2}{\sqrt{5}}$	$-\sqrt{2}v$	$-2v$	$-\sqrt{2}v$	$\frac{v^2-v}{2}\frac{2}{\sqrt{5}}$
$\frac{v^2-v}{2}\frac{1}{\sqrt{2}}$	$\frac{v^2-v}{2}\frac{2}{\sqrt{5}}$	$\frac{v^2-v}{2}$	$\frac{v^2-v}{2}\frac{2}{\sqrt{5}}$	$\frac{v^2-v}{2}\frac{1}{\sqrt{2}}$

Output the filtered original image with the mask

Stop

Figure 3.2: Procedure of image enhancement using adaptive fractional differential method with the proposed mask

order method can extract only the edges, it strongly vanishes weak textures and smooth areas in the image. In other words, the 1-order method extracts a large amount of marginal information, but weak textures and smooth areas are severely reduced, making it hard to see the complete structure of the image. Thus, the enhancement effects of the traditional fractional differential methods are not desirable. The original AFDA comprehensively considered global and local information in medical images and yielded better enhancement effects than the existing image processing methods. Thus, in this section, instead of comparing with the existing methods as mentioned above, we only compare the effect of image enhancement of the improved AFDA with the new mask with the original AFDA.
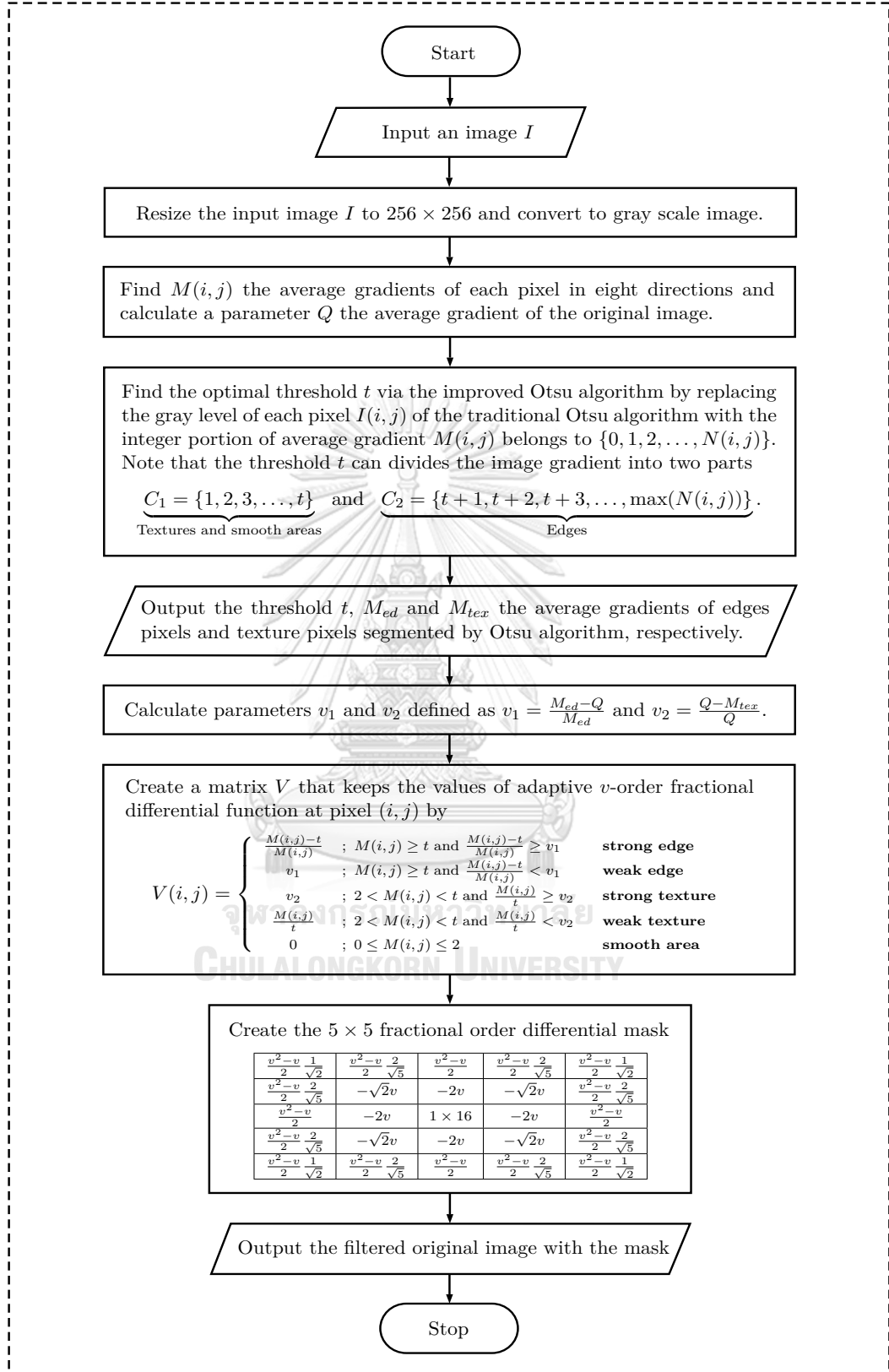
3.2.1 Evaluation by visual analysis

The original images (Figures 3.3(a) - 3.6(a)) have a low resolution and significant amounts of noise. Figures 3.3(b - c) - 3.6(b - c) show that the original AFDA and the improved AFDA with the new mask have enhanced the original image to some extent. Both of methods can enhance image edges and preserve weak textures and smooth areas concurrently. Considering both global and local information, the images processed by the improved AFDA with the new mask look clearer with weak textures and smooth areas preserved more appropriately. On the other hand, the images processed by the original AFDA sometimes look too sharp with undesirable noises (indicated by circles). Moreover, we find that there are some black and white spots appear in the images processed by the original AFDA (indicated by boxes) that do not occur on the original image. This effect is improper for medical image enhancement. Therefore, the improved AFDA with the new mask visually produces better medical image enhancement than the original AFDA with higher adaptability and more appropriate.

3.2.2 Evaluation by edge detection

The validation of the improvement can also be assessed by the quality of the edge detection. We use the Sobel and Laplacian operators to create an image emphasizing edges. They are commonly used as edge detection schemes. The Sobel and Laplacian

(*a*) Original image   (*b*) Original AFDA   (*c*) Improved AFDA
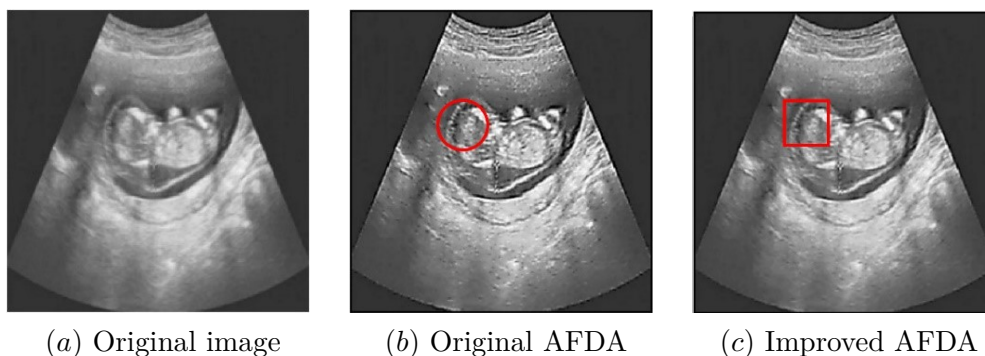
Figure 3.3: Type-B ultrasound image enhancement

(*a*) Original image   (*b*) Original AFDA   (*c*) Improved AFDA
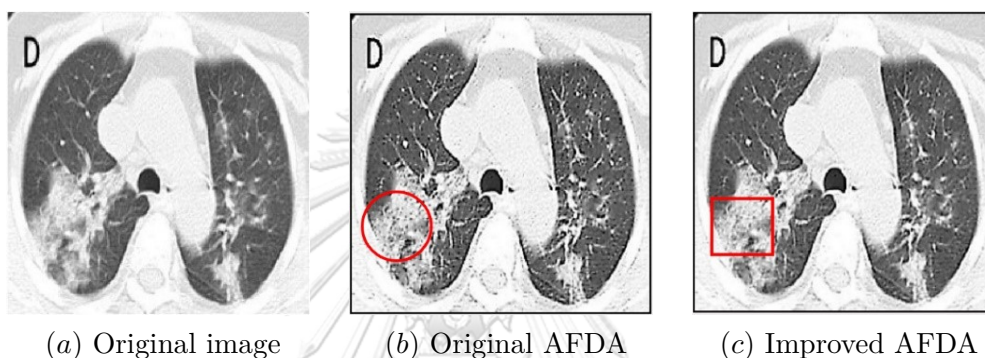
Figure 3.4: CT image enhancement

(*a*) Original image   (*b*) Original AFDA   (*c*) Improved AFDA
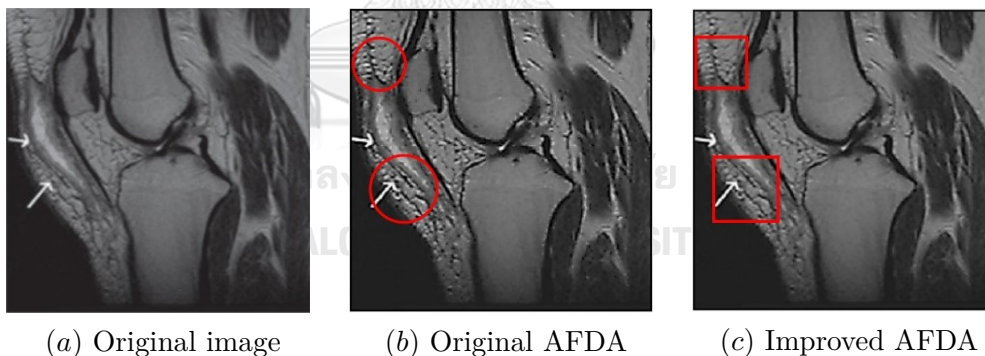
Figure 3.5: MRI image enhancement

operators are the gradient based edge detector and the Laplacian based edge detector, respectively. In other words, the Sobel and Laplacian operators are first-order and second-order linear differential operators, respectively. They can strongly enhance edges while strongly weaken weak textures and smooth areas of an image. We use the CT and MRI images as examples to compare the quality of the edge detection.

(*a*) Original image   (*b*) Original AFDA   (*c*) Improved AFDA
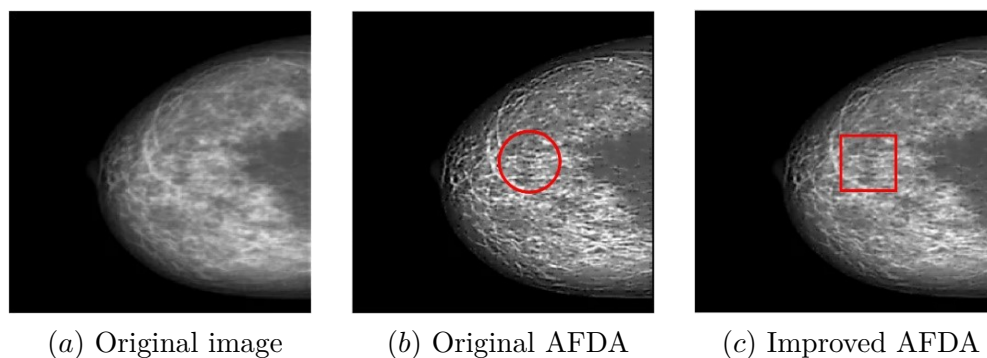
Figure 3.6: Target of breast molybdenum image enhancement

(*a*) Original image   (*b*) Original AFDA   (*c*) Improved AFDA
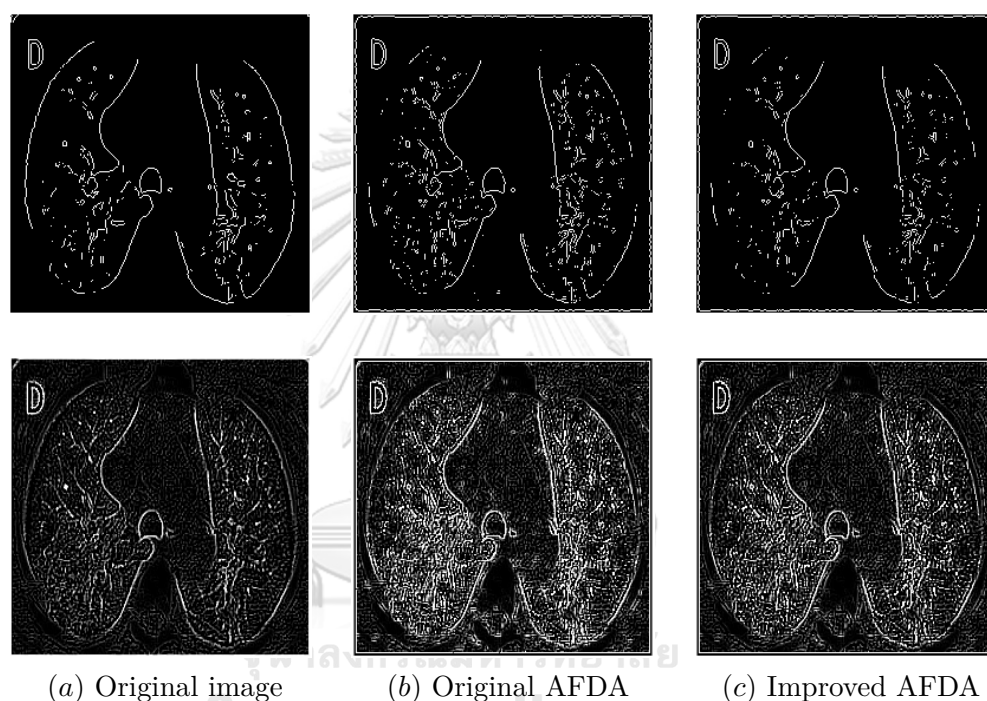
Figure 3.7: Edge detection results of CT images using Sobel(top) and Laplacian(bottom)

Figures 3.7 and 3.8 show the effect of image segmentation. The original AFDA and the improved AFDA with the new mask are shown to be significantly better than that of the original image. However, the edges enhanced by the original AFDA method is too sharp because the gradient has been given over-valuation by the original 8-direction mask. The improved AFDA with the new mask is shown to yield the better edge detection quality.

(a) Original image   (b) Original AFDA   (c) Improved AFDA
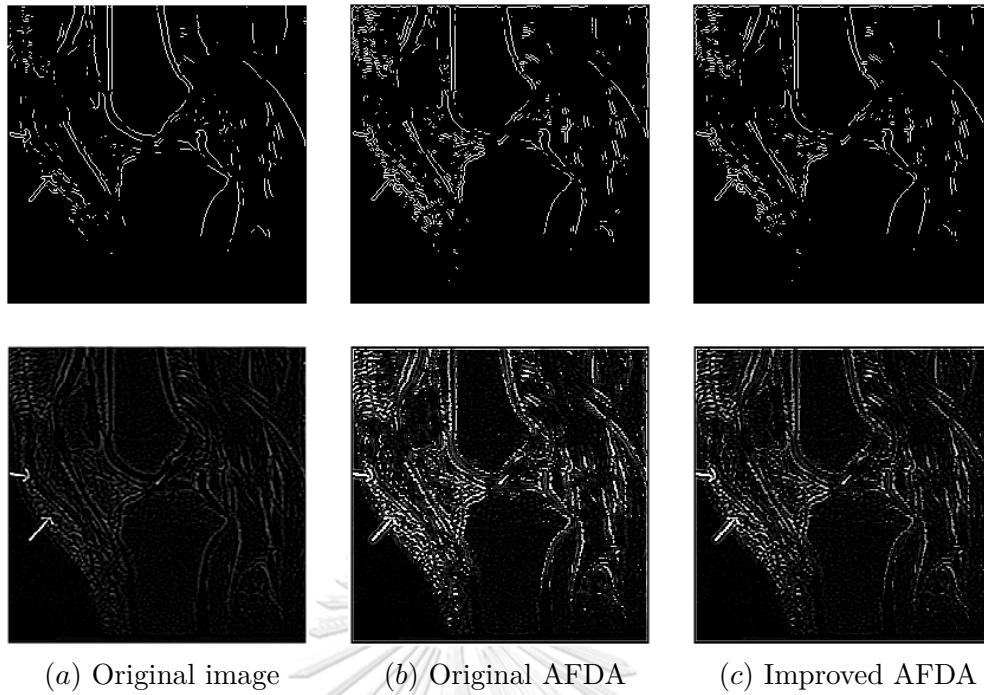
Figure 3.8: Edge detection results of MRI images using Sobel (top) and Laplacian (bottom)

3.2.3 Evaluation by some metrics

Finally, we use 5 metrics, namely the proportion of edge pixels, the average gradients of edge pixels, the average grays of texture pixels, the information entropy and the contrast ratio to analyze the effect of image enhancement using the improved AFDA with the new mask.

The proportion of edge pixels, the average gradients of edge pixels and the average grays of texture pixels can be obtained from the improved Otsu algorithm. Here, the definition of contrast ratio is $Contrast ratio = C_{processed}/C_{original}$, where $C_{original}$ and $C_{processed}$ are the contrast of the image before and after being processed, respectively. We consider 3×3 pixels to be a unit of an image. The parameter C is the average contrast of all 3×3 units. The evaluation parameters are given in Tables 3.2 - 3.5.

Type/parameter	Proportion of edge pixels	Average gradient of edge pixels	Average gray of texture pixels	Entropy of information	Contrast ratio
Original image	0.1188	9.4547	99.1850	6.4804	1.0000
Original AFDA	0.1410	37.3990	95.9056	6.6147	1.4607
Improved AFDA	0.1663	23.0451	98.0728	6.6195	1.3416

Table 3.2: The evaluation parameters of the ultrasonic image

Type/parameter	Proportion of edge pixels	Average gradient of edge pixels	Average gray of texture pixels	Entropy of information	Contrast ratio
Original image	0.1149	22.3739	192.6722	6.9584	1.0000
Original AFDA	0.1365	82.1330	188.4240	6.7774	1.5560
Improved AFDA	0.1329	65.1363	187.7429	6.9197	1.4420

Table 3.3: The evaluation parameters of the lung sectional CT image

Type/parameter	Proportion of edge pixels	Average gradient of edge pixels	Average gray of texture pixels	Entropy of information	Contrast ratio
Original image	0.0962	10.9120	81.0635	6.6909	1.0000
Original AFDA	0.1238	37.4280	77.9944	6.8983	1.6103
Improved AFDA	0.1250	24.8553	78.4106	6.8430	1.5370

Table 3.4: The evaluation parameters of the knee-joint MRI image

Type/parameter	Proportion of edge pixels	Average gradient of edge pixels	Average gray of texture pixels	Entropy of information	Contrast ratio
Original image	0.1357	7.0911	43.6800	4.8078	1.0000
Original AFDA	0.1489	36.1885	42.0671	4.8315	2.3445
Improved AFDA	0.1318	22.5202	43.7205	4.7926	2.2659

Table 3.5: The evaluation parameters of the target of breast molybdenum image

From Tables 3.2 - 3.5, the improved AFDA with the new mask can enhance the proportion of edge pixels significantly better than the original AFDA in the ultrasonic image. However, the proposed mask produces no different the proportion of edge pixels in enhancing the lung sectional CT image and the knee-joint MRI image to the original AFDA. Although, the new mask has less proportion of edge pixels than the original AFDA in the target of breast molybdenum image, the improved AFDA has the average gray of texture pixels higher and has the entropy of information closer to the entropy of the original image than the original AFDA which indicate that the improved AFDA with

the new mask can preserve the weak textures more appropriate than the original AFDA. The average gradient of edge pixels of every processed images by the improved AFDA is significantly less than using the original AFDA because of the assigned weight in the proposed mask. The closer entropy of images show that images processed by the improve AFDA with the new mask have a similar information quality to that of the original images more than the original AFDA. In addition, the average gradient of edge pixels and the contrast ratio are considerably increase from the original image but still less than the original AFDA which indicate that the improved AFDA with the new mask can enhance the edges looking not too sharp.

3.3 Conclusion

In this chapter, we propose a construction of the new 5×5 fractional order differential mask that uses sixteen directions of gradient operator and weights each pixel in the mask by the Euclidean distance from the center of the mask to reduce the over-valuation of the gradient from distant pixels. We performed both quantitative and qualitative comparative analysis with existing edge detectors and some metrics, respectively. From quantitative analysis, it is observed that an improvement of information entropy of image through the improved AFDA with the new mask is more than the original AFDA, thus enhancing more textural information. The proposed mask can improve the visual quality of images while preserving more information in medical images and improving the clarity and contrast of medical images. In addition, we find that there are some black and white spots appear in the images processed by the original AFDA method that do not occur on the original image. This effect is improper for medical image enhancement. Therefore, the improved AFDA with the new mask visually produces better medical image enhancement than other methods with higher adaptability and more appropriate which help doctors to diagnose illness more efficiently and accurately.

3.4 Comparison of masks

From our proposed method, we both include more directions and apply some weights to our new fractional differential mask used for enhancing the image. To see more clearly

whether directions or weights has more effect to the enhancement, we perform these two experiments. Here, we denote the original mask of eight directions by Mask 0, the mask of eight directions with applying weight by Mask 1, the mask of sixteen directions without applying weight by Mask 2 and the mask of sixteen directions with applying weight by Mask 3. These four masks are shown in Figure 3.9.

Experiment 1 Using the mask of eight directions proposed by Li and Xie [15] with applying weight due to the Euclidean distance from the center, we have the following results.

According to Figures 3.10(b - c) -3.13(b - c), Mask 1 produces the processed images which can preserve more texture better than Mask 0 as a result of applying weights. In addition, Mask 1 visually gives the processed images as same as Mask 3, see Figures 3.10(c and e) - 3.13(c and e). Moreover, five metrics in Tables 3.6 - 3.9 also support these conclusions because Mask 1 has these five metrics very similar to Mask 3 and Mask 3 provides a better enhancement than Mask 0 as we discussed in the previous section. Thus, applying weights has more effect to the enhancement than increasing the directions.

Experiment 2 Using the mask of sixteen directions without applying weight due to the Euclidean distance from the center, we have the following results.

From the experimental result, Mask 2 visually gives the processed images as same as Mask 0 as shown in Figures 3.10(b and d) - 3.13(b and d). However, Mask 3 produces the processed images which can preserve more texture better than Mask 2 as a result of applying weights as shown in Figures 3.10(b - c) -3.13(b - c). Moreover, five metrics in Tables 3.6 - 3.9 also confirm these conclusions because Mask 2 has these five metrics very similar to Mask 0 and Mask 3 provides a better enhancement than Mask 0 as we discussed in the previous section. Thus, adding a direction has almost no performance gain.

(a) Mask 0

$\frac{v^2-v}{2}$	0	$\frac{v^2-v}{2}$	0	$\frac{v^2-v}{2}$
0	$-v$	$-v$	$-v$	0
$\frac{v^2-v}{2}$	$-v$	1×8	$-v$	$\frac{v^2-v}{2}$
0	$-v$	$-v$	$-v$	0
$\frac{v^2-v}{2}$	0	$\frac{v^2-v}{2}$	0	$\frac{v^2-v}{2}$

(b) Mask 1

$\frac{v^2-v}{2}\cdot\frac{2}{2\sqrt{2}}$	0	$\frac{v^2-v}{2}$	0	$\frac{v^2-v}{2}\cdot\frac{2}{2\sqrt{2}}$
0	$-v\cdot\frac{1}{\sqrt{2}}$	$-v$	$-v\cdot\frac{1}{\sqrt{2}}$	0
$\frac{v^2-v}{2}$	$-v$	1×8	$-v$	$\frac{v^2-v}{2}$
0	$-v\cdot\frac{1}{\sqrt{2}}$	$-v$	$-v\cdot\frac{1}{\sqrt{2}}$	0
$\frac{v^2-v}{2}\cdot\frac{2}{2\sqrt{2}}$	0	$\frac{v^2-v}{2}$	0	$\frac{v^2-v}{2}\cdot\frac{2}{2\sqrt{2}}$

(c) Mask 2

$\frac{v^2-v}{2}$	$\frac{v^2-v}{2}$	$\frac{v^2-v}{2}$	$\frac{v^2-v}{2}$	$\frac{v^2-v}{2}$
$\frac{v^2-v}{2}$	$-2v$	$-2v$	$-2v$	$\frac{v^2-v}{2}$
$\frac{v^2-v}{2}$	$-2v$	1×16	$-2v$	$\frac{v^2-v}{2}$
$\frac{v^2-v}{2}$	$-2v$	$-2v$	$-2v$	$\frac{v^2-v}{2}$
$\frac{v^2-v}{2}$	$\frac{v^2-v}{2}$	$\frac{v^2-v}{2}$	$\frac{v^2-v}{2}$	$\frac{v^2-v}{2}$

(d) Mask 3

$\frac{v^2-v}{2}\cdot\frac{2}{2\sqrt{2}}$	$\frac{v^2-v}{2}\cdot\frac{2}{\sqrt{5}}$	$\frac{v^2-v}{2}\cdot\frac{2}{2}$	$\frac{v^2-v}{2}\cdot\frac{2}{\sqrt{5}}$	$\frac{v^2-v}{2}\cdot\frac{2}{2\sqrt{2}}$
$\frac{v^2-v}{2}\cdot\frac{2}{\sqrt{5}}$	$-2v\cdot\frac{1}{\sqrt{2}}$	$-2v\cdot\frac{1}{1}$	$-2v\cdot\frac{1}{\sqrt{2}}$	$\frac{v^2-v}{2}\cdot\frac{2}{\sqrt{5}}$
$\frac{v^2-v}{2}\cdot\frac{2}{2}$	$-2v\cdot\frac{1}{1}$	1×16	$-2v\cdot\frac{1}{1}$	$\frac{v^2-v}{2}\cdot\frac{2}{2}$
$\frac{v^2-v}{2}\cdot\frac{2}{\sqrt{5}}$	$-2v\cdot\frac{1}{\sqrt{2}}$	$-2v\cdot\frac{1}{1}$	$-2v\cdot\frac{1}{\sqrt{2}}$	$\frac{v^2-v}{2}\cdot\frac{2}{\sqrt{5}}$
$\frac{v^2-v}{2}\cdot\frac{2}{2\sqrt{2}}$	$\frac{v^2-v}{2}\cdot\frac{2}{\sqrt{5}}$	$\frac{v^2-v}{2}\cdot\frac{2}{2}$	$\frac{v^2-v}{2}\cdot\frac{2}{\sqrt{5}}$	$\frac{v^2-v}{2}\cdot\frac{2}{2\sqrt{2}}$

Figure 3.9: Four fractional differential masks

(a) Original image   (b) Mask 0   (c) Mask 1

(d) Mask 2   (e) Mask 3

Figure 3.10: Type-B ultrasound image enhancement
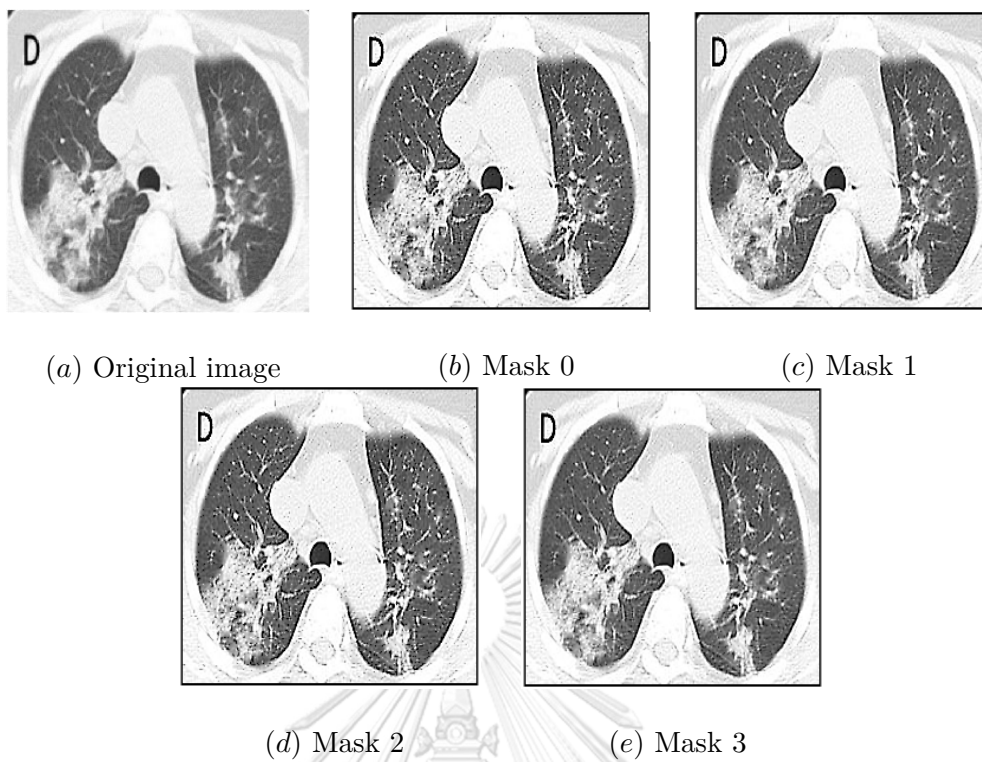
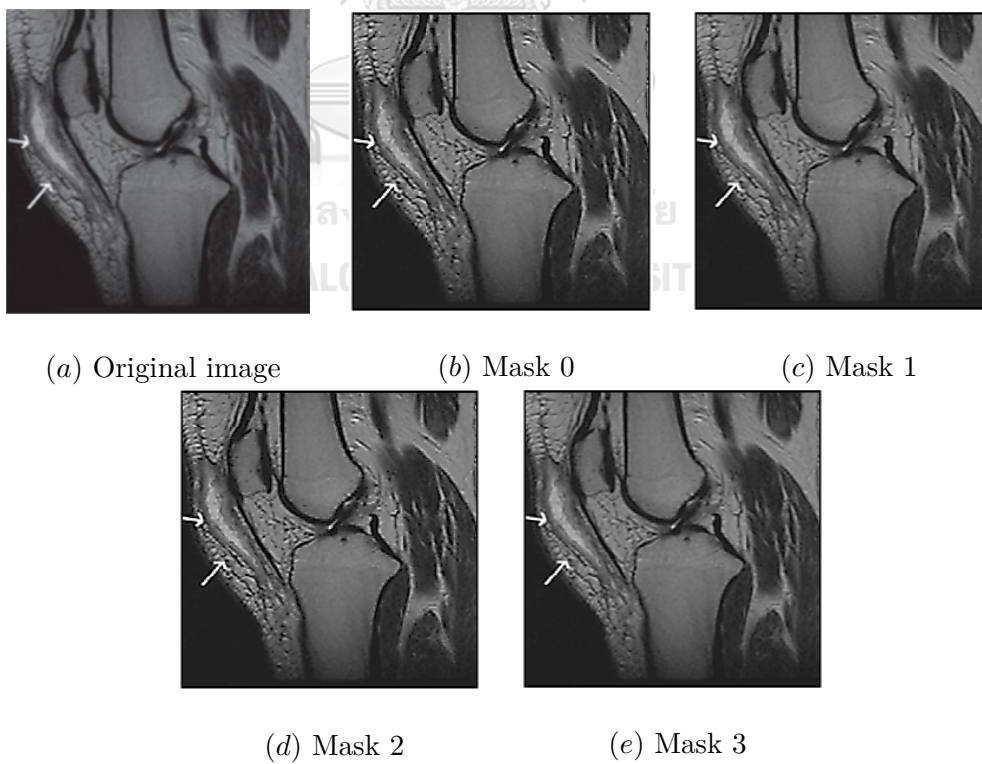(a) Original image   (b) Mask 0   (c) Mask 1

(d) Mask 2   (e) Mask 3

Figure 3.11: CT image enhancement

(a) Original image   (b) Mask 0   (c) Mask 1

(d) Mask 2   (e) Mask 3

Figure 3.12: MRI image enhancement

(a) Original image   (b) Mask 0   (c) Mask 1
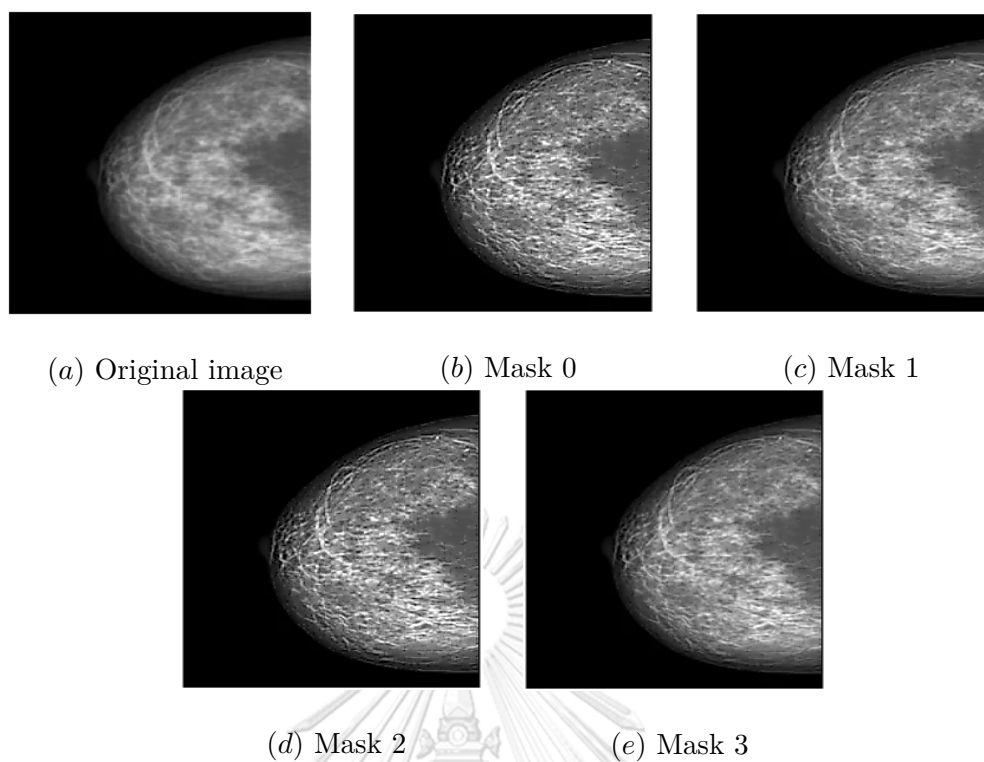
(d) Mask 2   (e) Mask 3

Figure 3.13: Target of breast molybdenum image enhancement

Type/parameter	Proportion of edge pixels	Average gradient of edge pixels	Average gray of texture pixels	Entropy of information	Contrast ratio
Original image	0.1188	9.4547	99.1850	6.4804	1.0000
Mask 0	0.1410	37.3990	95.9056	6.6147	1.4607
Mask 1	0.1658	22.9269	98.0925	6.6192	1.3352
Mask 2	0.1405	37.4720	95.9436	6.6151	1.4671
Mask 3	0.1663	23.0451	98.0728	6.6195	1.3416

Table 3.6: The evaluation parameters of the ultrasonic image

Type/parameter	Proportion of edge pixels	Average gradient of edge pixels	Average gray of texture pixels	Entropy of information	Contrast ratio
Original image	0.1149	22.3739	192.6722	6.9584	1.0000
Mask 0	0.1365	82.1330	188.4240	6.7774	1.5560
Mask 1	0.1346	64.4145	187.7967	6.9200	1.4416
Mask 2	0.1366	82.2524	188.4213	6.7775	1.5616
Mask 3	0.1329	65.1363	187.7429	6.9197	1.4420

Table 3.7: The evaluation parameters of the lung sectional CT image

Type/parameter	Proportion of edge pixels	Average gradient of edge pixels	Average gray of texture pixels	Entropy of information	Contrast ratio
Original image	0.0962	10.9120	81.0635	6.6909	1.0000
Mask 0	0.1238	37.4280	77.9944	6.8983	1.6103
Mask 1	0.1248	24.7189	78.4078	6.8418	1.5485
Mask 2	0.1233	37.4516	78.0071	6.8983	1.6093
Mask 3	0.1250	24.8553	78.4106	6.8430	1.5370

Table 3.8: The evaluation parameters of the knee-joint MRI image

Type/parameter	Proportion of edge pixels	Average gradient of edge pixels	Average gray of texture pixels	Entropy of information	Contrast ratio
Original image	0.1357	7.0911	43.6800	4.8078	1.0000
Mask 0	0.1489	36.1885	42.0671	4.8315	2.3445
Mask 1	0.1444	21.4870	42.6308	4.7923	2.2512
Mask 2	0.1484	36.3062	42.1070	4.8314	2.3450
Mask 3	0.1318	22.5202	43.7205	4.7926	2.2659

Table 3.9: The evaluation parameters of the target of breast molybdenum image

3.5 Future work

In this work, we proposed the new 5×5 fractional order differential mask. It is interesting to study the new one of the size 7×7 because it has to use more coefficient terms of the approximation of the fractional differential and can extend the direction more than sixteen directions. Moreover, if we can recruit some expert medical doctors who can give us some feedback on our results after we obtain the new enhanced image, our algorithm should be strongly reliable.
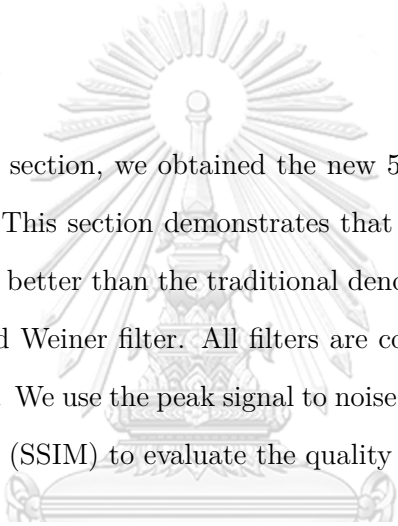
CHAPTER IV

IMAGE DENOISING USING AN IMPROVED MASK

In this chapter, we apply the proposed mask to restore the noisy images which are corrupted by the Gaussian noise to provide other evidence that the proposed mask has an influence on preserving more texture detail.

4.1 Introduction

From the previous section, we obtained the new 5×5 fractional differential mask as shown in Figure 4.1. This section demonstrates that a denoising algorithm using the proposed mask performs better than the traditional denoising filters which contain mean filter, Gaussian filter and Weiner filter. All filters are considered to operate using 5×5 processing window mask. We use the peak signal to noise ratio (PSNR) and the structural similarity index measure (SSIM) to evaluate the quality of the denoised images.

$\frac{v^2 - v}{2} \cdot \frac{2}{2\sqrt{2}}$	$\frac{v^2 - v}{2} \cdot \frac{2}{\sqrt{5}}$	$\frac{v^2 - v}{2} \cdot \frac{2}{2}$	$\frac{v^2 - v}{2} \cdot \frac{2}{\sqrt{5}}$	$\frac{v^2 - v}{2} \cdot \frac{2}{2\sqrt{2}}$
$\frac{v^2 - v}{2} \cdot \frac{2}{\sqrt{5}}$	$-2v \cdot \frac{1}{\sqrt{2}}$	$-2v \cdot \frac{1}{1}$	$-2v \cdot \frac{1}{\sqrt{2}}$	$\frac{v^2 - v}{2} \cdot \frac{2}{\sqrt{5}}$
$\frac{v^2 - v}{2} \cdot \frac{2}{2}$	$-2v \cdot \frac{1}{1}$	1×16	$-2v \cdot \frac{1}{1}$	$\frac{v^2 - v}{2} \cdot \frac{2}{2}$
$\frac{v^2 - v}{2} \cdot \frac{2}{\sqrt{5}}$	$-2v \cdot \frac{1}{\sqrt{2}}$	$-2v \cdot \frac{1}{1}$	$-2v \cdot \frac{1}{\sqrt{2}}$	$\frac{v^2 - v}{2} \cdot \frac{2}{\sqrt{5}}$
$\frac{v^2 - v}{2} \cdot \frac{2}{2\sqrt{2}}$	$\frac{v^2 - v}{2} \cdot \frac{2}{\sqrt{5}}$	$\frac{v^2 - v}{2} \cdot \frac{2}{2}$	$\frac{v^2 - v}{2} \cdot \frac{2}{\sqrt{5}}$	$\frac{v^2 - v}{2} \cdot \frac{2}{2\sqrt{2}}$

Figure 4.1: The proposed 5×5 fractional differential mask

4.2 Experiment, Results and Discussion

The test images employed here are the grayscale images "Peacock" and "Satellite" with 512×512 pixels as shown in Figures 4.2(a)-4.9(a). The Gaussian noise with a mean of zero is added into the image with different variance values $0.01, 0.03, 0.05$ and 0.10 as shown in Figures 4.2(b)-4.9(b). We do not consider the Gaussian noise of variance values greater than 0.10 because we consider those levels of variances cause the image to be overly damaged, making it irreparable. Tables 4.2-4.9 show the PSNR, SSIM and PSNR*SSIM values.

The values of the fractional order of the proposed mask are taken with the negative sign because each element of the proposed mask becomes non-negative for the propose of being a smoothing filter. In this experiment, we considered values of v from -0.1 to -8 with a decrement -0.1. Table 4.1 shows the fractional orders v of the proposed filter that we used for each image which obtained by maximizing the PSNR*SSIM. We performed both qualitative and quantitative analysis to evaluate the quality of the denoised images using the peak signal to noise ratio (PSNR) and the structural similarity index measure (SSIM). The experimental results are shown in Figures 4.2-4.9 and Tables 4.2-4.9.

Image	Variance of Gaussiance noise	Fractional order v
Peacock	0.01	-0.5
	0.03	-0.9
	0.05	-1.1
	0.10	-1.3
Satellite	0.01	-0.5
	0.03	-0.7
	0.05	-0.9
	0.10	-1.1

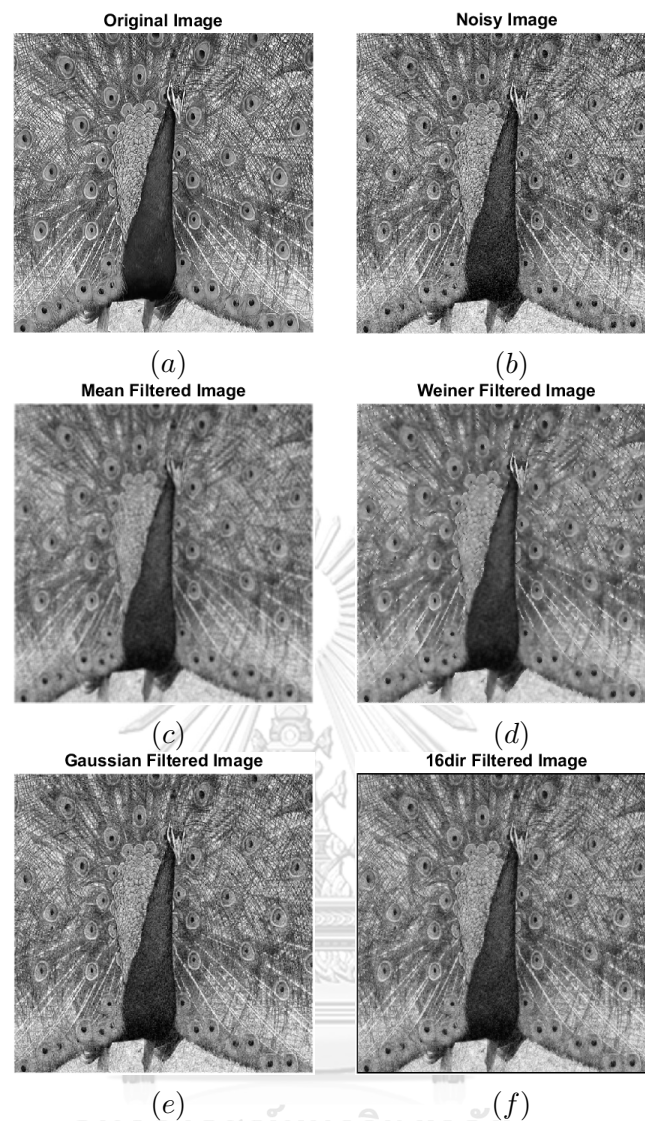**Table 4.1:** Fractional order for each image

Figure 4.2: Comparison the denoised peacock images which corrupted by Gaussian noise with variance 0.01

Metric/Type	Original	Noisy	Mean	Weiner	Gaussian	Proposed
PSNR	∞	16.1444	17.3515	17.5880	17.1519	16.6569
SSIM	1	0.3970	0.2905	0.3474	0.4355	0.4234
PSNR*SSIM	∞	6.4093	5.0406	6.1101	7.4697	7.0525

Table 4.2: Comparison of PSNR and SSIM of denoised peacock images which corrupted by Gaussian noise with variance 0.01
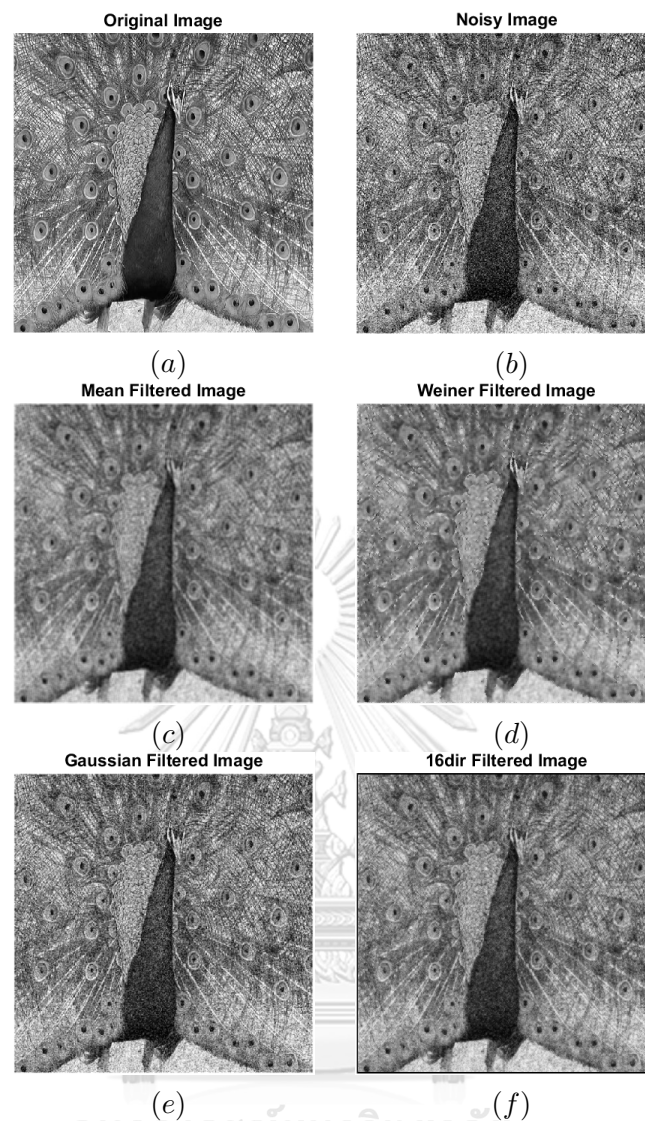
Figure 4.3: Comparison the denoised peacock images which corrupted by Gaussian noise with variance 0.03

Metric/Type	Original	Noisy	Mean	Weiner	Gaussian	Proposed
PSNR	∞	14.8280	17.1548	17.2937	16.1852	16.4064
SSIM	1	0.3076	0.2710	0.3175	0.3574	0.3610
PSNR*SSIM	∞	4.5611	4.6490	5.4908	5.7846	5.9227

Table 4.3: Comparison of PSNR and SSIM of denoised peacock images which corrupted by Gaussian noise with variance 0.03
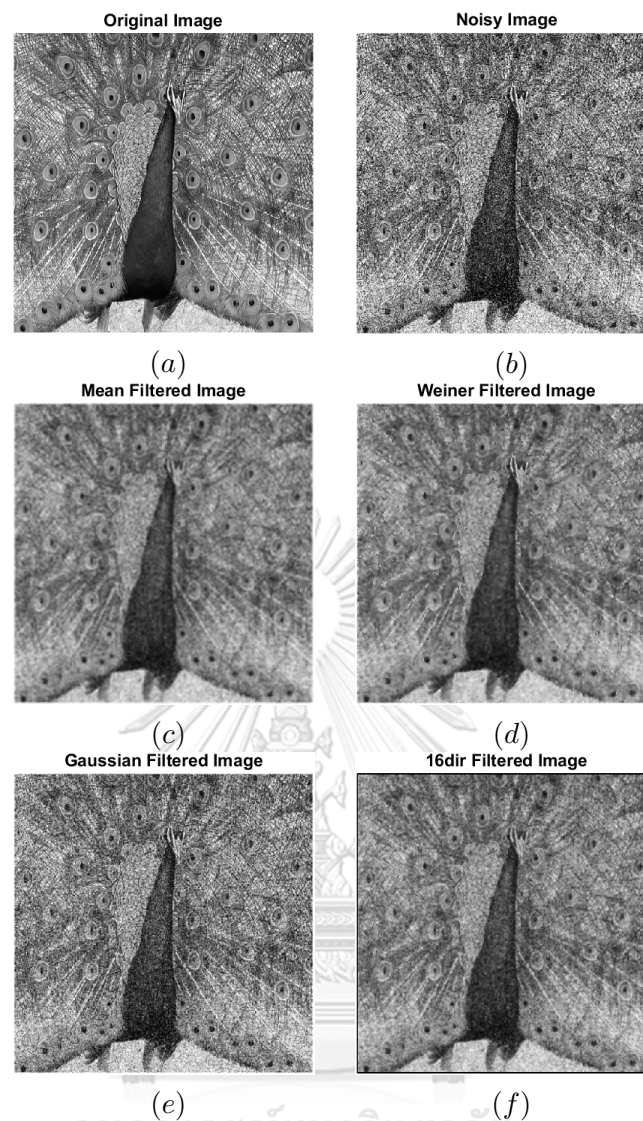
Figure 4.4: Comparison the denoised peacock images which corrupted by Gaussian noise with variance 0.05

Metric/Type	Original	Noisy	Mean	Weiner	Gaussian	Proposed
PSNR	∞	13.9338	16.9596	17.0412	15.4743	16.1600
SSIM	1	0.2575	0.2543	0.2933	0.3093	0.3247
PSNR*SSIM	∞	3.5880	4.3128	4.9982	4.7862	5.2472

Table 4.4: Comparison of PSNR and SSIM of denoised peacock images which corrupted by Gaussian noise with variance 0.05
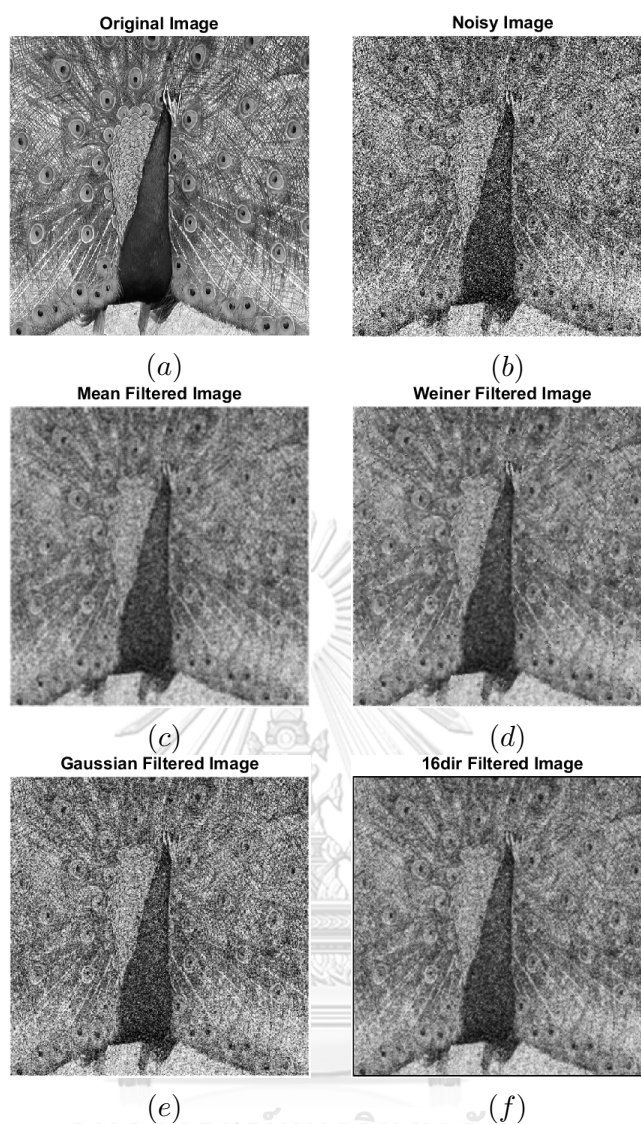
Figure 4.5: Comparison the denoised peacock images which corrupted by Gaussian noise with variance 0.10

Metric/Type	Original	Noisy	Mean	Weiner	Gaussian	Proposed
PSNR	∞	12.6257	16.5701	16.5578	14.3645	15.6911
SSIM	1	0.1938	0.2255	0.2515	0.2431	0.2731
PSNR*SSIM	∞	2.4469	3.7366	4.1643	3.4920	4.2852

Table 4.5: Comparison of PSNR and SSIM of denoised peacock images which corrupted by Gaussian noise with variance 0.10
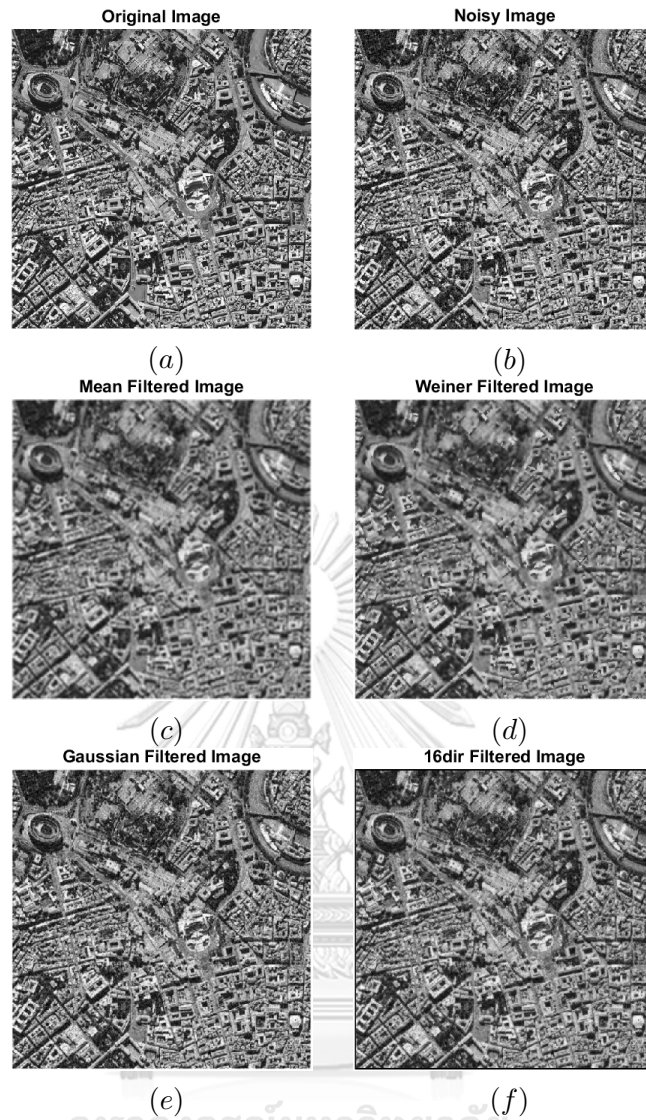
Figure 4.6: Comparison the denoised satellite images which corrupted by Gaussian noise with variance 0.01

Metric/Type	Original	Noisy	Mean	Weiner	Gaussian	Proposed
PSNR	∞	15.2165	15.8807	16.1836	16.0341	16.1424
SSIM	1	0.5470	0.4289	0.4804	0.5806	0.5685
PSNR*SSIM	∞	8.3234	6.8112	7.7746	9.3094	9.1770

Table 4.6: Comparison of PSNR and SSIM of denoised satellite images which corrupted by Gaussian noise with variance 0.01
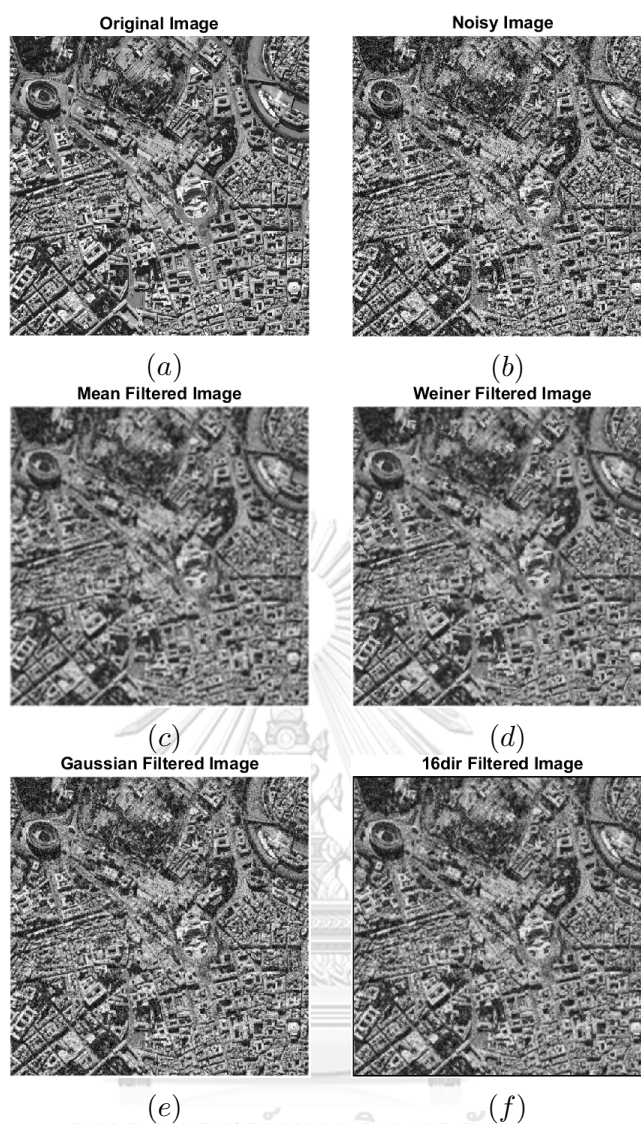
Figure 4.7: Comparison the denoised satellite images which corrupted by Gaussian noise with variance 0.03

Metric/Type	Original	Noisy	Mean	Weiner	Gaussian	Proposed
PSNR	∞	14.2180	15.6828	15.9303	15.3260	15.7638
SSIM	1	0.4650	0.4091	0.4546	0.5158	0.5149
PSNR*SSIM	∞	6.6114	6.4158	7.2419	7.9052	8.1168

Table 4.7: Comparison of PSNR and SSIM of denoised satellite images which corrupted by Gaussian noise with variance 0.03
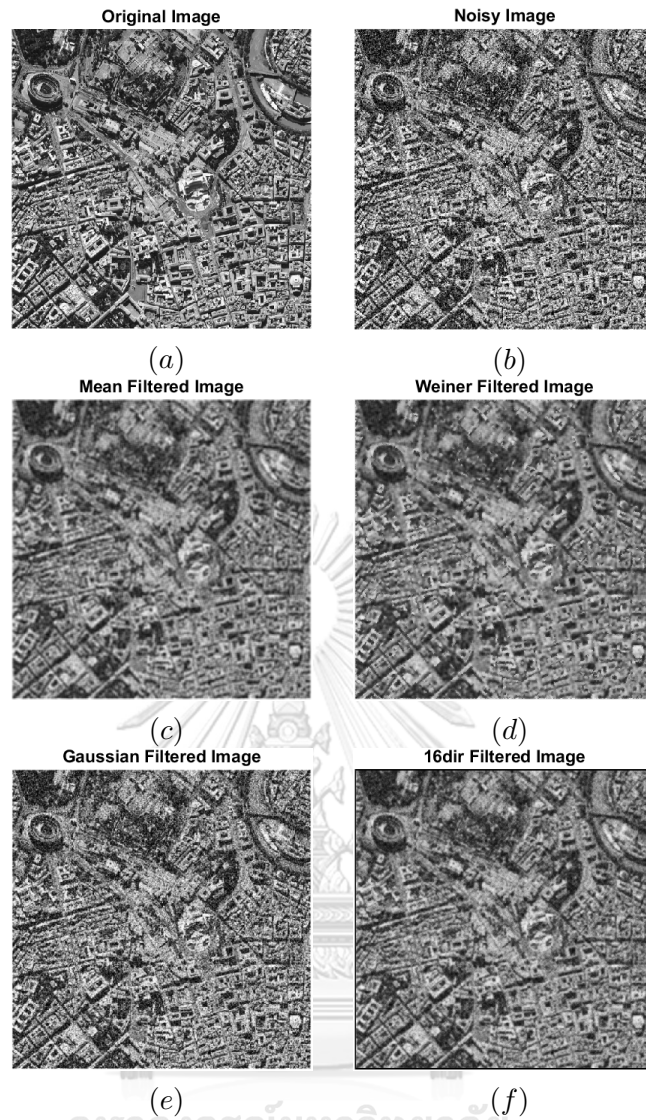
Figure 4.8: Comparison the denoised satellite images which corrupted by Gaussian noise with variance 0.05

Metric/Type	Original	Noisy	Mean	Weiner	Gaussian	Proposed
PSNR	∞	13.5198	15.5118	15.7124	14.7874	15.5245
SSIM	1	0.4126	0.3926	0.4330	0.4703	0.4794
PSNR*SSIM	∞	5.5783	6.0899	6.8035	6.9545	7.4424

Table 4.8: Comparison of PSNR and SSIM of denoised satellite images which corrupted by Gaussian noise with variance 0.05
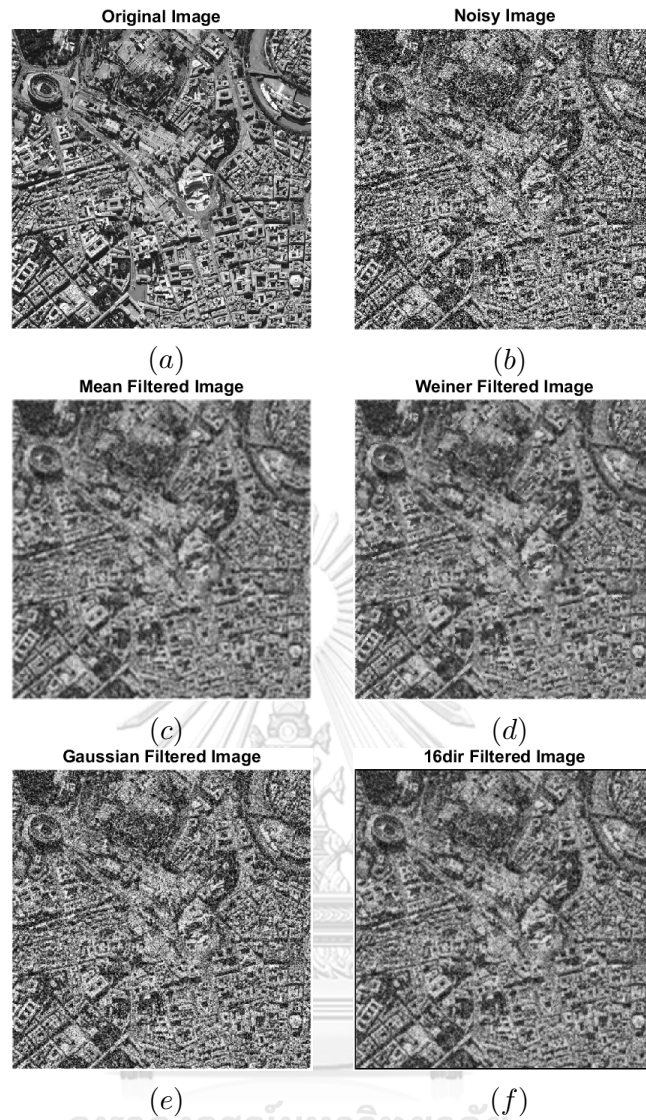
Figure 4.9: Comparison the denoised satellite images which corrupted by Gaussian noise with variance 0.10

Metric/Type	Original	Noisy	Mean	Weiner	Gaussian	Proposed
PSNR	∞	12.3698	15.1147	15.2594	13.8462	14.9964
SSIM	1	0.3313	0.3590	0.3910	0.3948	0.4213
PSNR*SSIM	∞	4.0981	5.4262	5.9664	5.4665	6.3180

Table 4.9: Comparison of PSNR and SSIM of denoised satellite images which corrupted by Gaussian noise with variance 0.10

Figures 4.2(c)-4.9(c) and Figures 4.2(d)-4.9(d) show the image processed by mean filter and Weiner filter, respectively, in which there is a significant blurring. Figures 4.2(f)-4.9(f) illustrate that the image processed by the proposed filter has a good denoising performance for both testing images by different degrees of noise, in which there is no significant blurring and the texture information has been well preserved. When the image corrupted by Gaussian noise with very low level of variance as 0.01, the Gaussian filter can perform a better result as shown in Figures 4.2(e) and 4.6(e) and the values of both PSNR and SSIM of Gaussian filter is the highest among the other filters as shown in Tables 4.2 and 4.6, respectively. However, when the image is corrupted by Gaussian noise with higher levels of variance as $0.03, 0.05$ and 0.10, the proposed filter has a better denoising performance than the others which can be indicated by a higher PSNR higher SSIM and higher PSNR*SSIM as shown in Figures 4.3(f)-4.5(f), Figures 4.7(f)-4.9(f), Tables 4.3-4.5 and Tables 4.7-4.9, respectively. These results indicate that the proposed filter can robustly denoise the image while preserving its detailed features.

The proposed filter for image denoising provides satisfactory results. According to the assumption that higher PSNR indicates a better ability to eliminate the noise while higher SSIM indicates a better performance to carry important information about the structure of the objects in the visual scene, the highest PSNR*SSIM value of the proposed mask acts as one of the important parameters to judge its performance. In other words, the proposed filter well eliminates the noise while the output images have no significant blurring.

However, in practice we do not have a noise-free image to calculate the PSNR and the SSIM, so there is a problem that is what is an optimal order v that should be used for each image. Since each image has its characteristics, so it would be complex work to find out a formula of an optimal order v. To make it simple, we focus to find a range of the order v that should be used under the assumption that if the image has a similar characteristic, a similar order value should be used.

In this experiment, we consider two datasets of the medical images which are the

grayscale images of the 500 chest X-ray images and the 500 retinal OCT images (optical coherence tomography) with 512×512 pixels, some of them are shown in Figures 4.10(a) and 4.11(a). For each original image, the Gaussian noise with a mean of zero is added into those images with variance 0.05 to generate the noisy images, an example of them is shown in Figures 4.10(b) and 4.11(b).
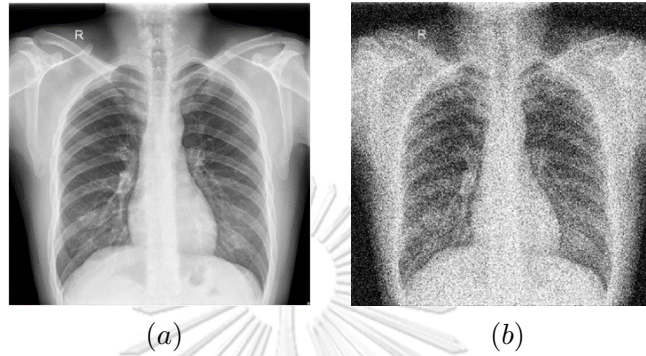

(a) $\qquad\qquad\qquad\qquad$ (b)

Figure 4.10: Original image and noisy image of chest X-ray image, respectively

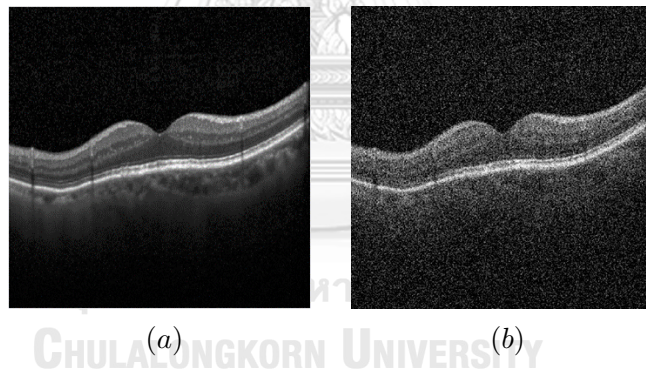(a) $\qquad\qquad\qquad\qquad$ (b)

Figure 4.11: Original image and noisy image of retinal OCT image, respectively

For each noisy image, we considered values of the fractional order v from -0.1 with a decrement -0.1. For each order v, we smooth the noisy image with the proposed filter and plot PSNR, SSIM and PSNR*SSIM against the orders v. The order v that has the highest values of PSNR, SSIM and PSNR*SSIM are collected. For example, the noisy chest X-ray the retinal OCT and in Figure 4.10 and Figure 4.11 have the plots as shown in Figure 4.12 and Figure 4.13, respectively. From the plots, while decreasing the order v, the values of PSNR, SSIM and PSNR*SSIM continue to increase until they reach their
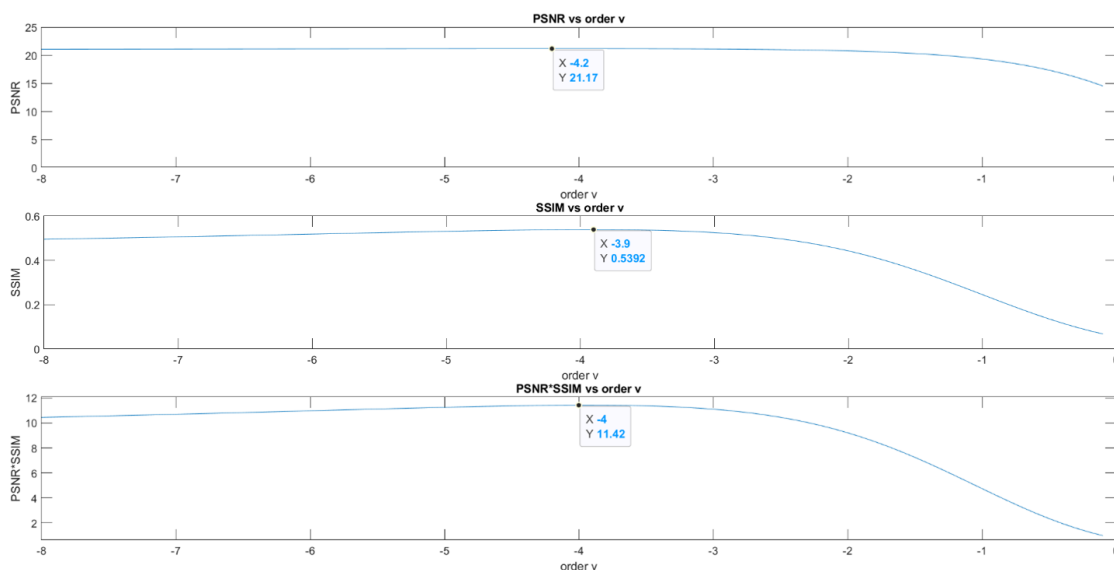
peak, and then they keep decreasing slowly.

Figure 4.12: The value of PSNR, SSIM and PSNR*SSIM for each order v of the noisy chest X-ray image in Figure 4.10
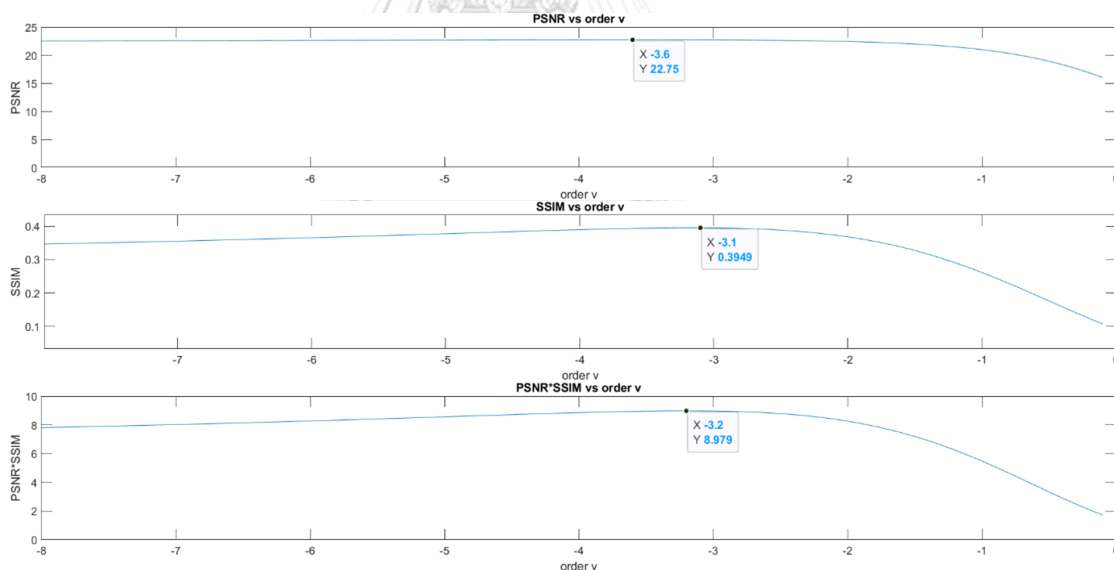

Figure 4.13: The value of PSNR, SSIM and PSNR*SSIM for each order v of the noisy retinal OCT image in Figure 4.11

After we perform this process to the 500 images of each dataset, we plot the histogram of the collected optimal orders v according to PSNR, SSIM and PSNR*SSIM, respectively, as shown in Figures 4.14 and 4.15. The range of the order v that should be

used can be obtained from the histogram. For example, from the histogram (c) in Figure 4.14, $[-4.1, -3.9]$ is a range of the fractional order v that should be used to smooth a noisy chest X-ray image which corrupted by the Gaussian noise with variance 0.05. From the histogram (c) in Figure 4.15, $[-4.5, -0.5]$ is a range of the fractional order v that should be used to smooth a noisy retinal OCT image which corrupted by the Gaussian noise with variance 0.05. In addition, we also calculate their mean and standard deviation as shown in Tables 4.10 and 4.11.
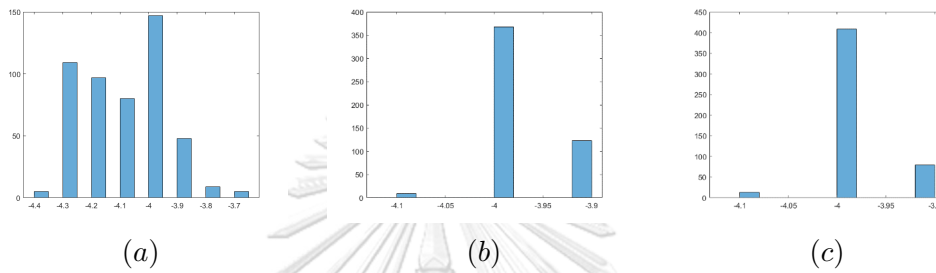

(a) (b) (c)

Figure 4.14: Histogram of the optimal orders v according to PSNR, SSIM and PSNR*SSIM, respectively, of the 500 chest X-ray images

Stat/Metric	PSNR	SSIM	PSNR*SSIM
Mean	-4.108	-3.9772	-3.9868
SD	0.1468	0.0461	0.0409

Table 4.10: Mean and standard deviation of the optimal orders v according to PSNR, SSIM and PSNR*SSIM, respectively, of the 500 chest X-ray images
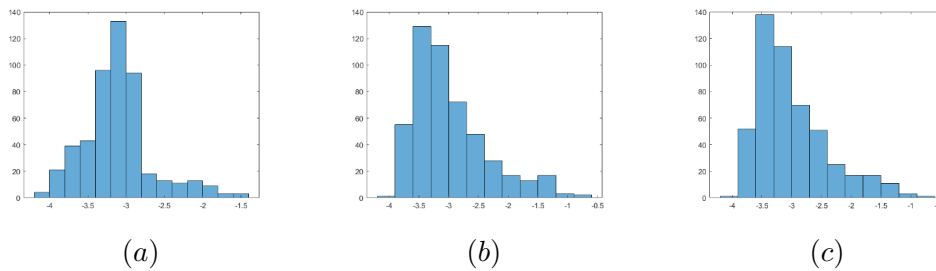

(a) (b) (c)

Figure 4.15: Histogram of the optimal orders v according to PSNR, SSIM and PSNR*SSIM, respectively, of the 500 retinal OCT images

Stat/Metric	PSNR	SSIM	PSNR*SSIM
Mean	-3.1542	-3.0302	-3.049
SD	0.4506	0.6230	0.5940

Table 4.11: Mean and standard deviation of the optimal orders v according to PSNR, SSIM and PSNR*SSIM, respectively, of the 500 retinal OCT images

4.3 Conclusion

In this chapter, we apply the proposed mask as a smoothing filter to perform an image denoising. Changing the values of the fractional orders will allow adjusting the filter coefficients to each image according to it characteristics. This makes the proposed filter to have a higher PSNR than mean filter, Weiner filter and Gaussian filter. Moreover, the experiments show that the proposed mask has a better denoising performance than the Gaussian filter when the image corrupted by Gaussian noise with a higher levels of variance. In addition, the proposed filter can preserve detailed features in rich texture images so that the output images have no significant blurring which can be indicated by higher SSIM. Thus, the proposed filter can improve the result visually and in terms of PSNR and SSIM efficiently.

4.4 Future work

In this work, the proposed method aim to obtain a range of an optimal order v for a specific noisy image because we do not have a noise-free image to calculate the PSNR and the SSIM. However, the limitation of this solution is that it need a large dataset to get the statistics together with computational cost. Therefore, we will find some way to obtain a formula of an optimal order v based on the characteristics of the image which could better deal with the limitation.

REFERENCES

[1] J. Lu, D. M. Healy Jr, and J. B. Weaver, "Contrast enhancement of medical images using multiscale edge representation," *Optical engineering*, vol. 33, no. 7, pp. 2151–2161, 1994.

[2] O. V. Michailovich and A. Tannenbaum, "Despeckling of medical ultrasound images," *ieee transactions on ultrasonics, ferroelectrics, and frequency control*, vol. 53, no. 1, pp. 64–78, 2006.

[3] X. Zong, A. F. Laine, and E. A. Geiser, "Speckle reduction and contrast enhancement of echocardiograms via multiscale nonlinear processing," *IEEE transactions on medical imaging*, vol. 17, no. 4, pp. 532–540, 1998.

[4] K. Oldham and J. Spanier, *The fractional calculus theory and applications of differentiation and integration to arbitrary order*. Elsevier, 1974.

[5] A. A. Kilbas, H. M. Srivastava, and J. J. Trujillo, *Theory and applications of fractional differential equations*, vol. 204. elsevier, 2006.

[6] C. Gao, J. Zhou, J. Hu, and F. Lang, "Edge detection of colour image based on quaternion fractional differential," *IET Image Processing*, vol. 5, no. 3, pp. 261–272, 2011.

[7] A. Nakib, Y. Schulze, and E. Petit, "Image thresholding framework based on two-dimensional digital fractional integration and legendre moments'," *IET image processing*, vol. 6, no. 6, pp. 717–727, 2012.

[8] Y.-F. Pu, J.-L. Zhou, and X. Yuan, "Fractional differential mask: a fractional differential-based approach for multiscale texture enhancement," *IEEE transactions on image processing*, vol. 19, no. 2, pp. 491–511, 2009.

[9] N. He, J.-B. Wang, L.-L. Zhang, and K. Lu, "An improved fractional-order differentiation model for image denoising," *signal Processing*, vol. 112, pp. 180–188, 2015.

[10] H. A. Jalab and R. W. Ibrahim, "Fractional masks based on generalized fractional differential operator for image denoising," *Int. J. Comput. Inf. Syst. Control Eng*, vol. 7, no. 2, pp. 169–174, 2013.

[11] C. Gao, J. Zhou, X. Zheng, and F. Lang, "Image enhancement based on improved fractional differentiation," *Journal of Computational Information Systems*, vol. 7, no. 1, pp. 257–264, 2011.

[12] B. Li and W. Xie, "Adaptive fractional differential algorithm based on otsu standard," in *The 26th Chinese Control and Decision Conference (2014 CCDC)*, pp. 2020–2025, IEEE, 2014.

[13] Y.-F. Pu and W. Wang, "Fractional differential masks of digital image and their numerical implementation algorithms," *Acta Automatica Sinica*, vol. 33, no. 11, pp. 1128–1135, 2007.

[14] W. Wang, W. Li, and X. Yu, "Fractional differential algorithms for rock fracture images," *The Imaging Science Journal*, vol. 60, no. 2, pp. 103–111, 2012.

[15] B. Li and W. Xie, "Adaptive fractional differential approach and its application to medical image enhancement," *Computers & Electrical Engineering*, vol. 45, pp. 324–335, 2015.

[16] R. C. Gonzalez, R. E. Woods, *et al.*, "Digital image processing," 2002.

[17] N. Otsu, "A threshold selection method from gray-level histograms," *IEEE transactions on systems, man, and cybernetics*, vol. 9, no. 1, pp. 62–66, 1979.

[18] D. H. Johnson, "Signal-to-noise ratio," *Scholarpedia*, vol. 1, no. 12, p. 2088, 2006.

[19] Z. Wang and A. C. Bovik, "Modern image quality assessment," *Synthesis Lectures on Image, Video, and Multimedia Processing*, vol. 2, no. 1, pp. 1–156, 2006.

[20] R. M. Gray, *Entropy and information theory*. Springer Science & Business Media, 2011.

BIOGRAPHY

Name   Mr. Wasin Tranghiranyathorn

Date of Birth   6 Jan 1996

Place of Birth   Trang, Thailand

Education   B.S. (Mathematics), Chulalongkorn University, 2018